ADVANCED OPTICAL MATERIALS
www.advopticalmat.de

Bright and Photostable TADF-Emitting Zirconium(IV) Pyridinedipyrrolide Complexes: Efficient Dyes for Decay Time-Based Temperature Sensing and Imaging

*Andreas Russegger, Angela C. Debruyne, Daniel Carvajal Berrio, Stefanie Fuchs, Julia Marzi, Katja Schenke-Layland, Ruslan I. Dmitriev, and Sergey M. Borisov**

Luminescence thermometry represents a technique of choice for measurements in small objects and imaging of temperature distribution. However, most state-of-the-art luminescent probes are limited in spectral characteristics, brightness, photostability, and sensitivity. Molecular thermometers of the new generation utilizing air and moisture-stable zirconium(IV) pyridinedipyrrolide complexes can address all these limitations. The dyes emit pure thermally activated delayed fluorescence without any prompt fluorescence and show a unique combination of attractive features: a) visible light excitation and emission in the orange/red region, b) high luminescence brightness (quantum yields ≈0.5 in toluene and 0.8–1.0 in polystyrene matrix), c) excellent photostability, d) suitability for two-photon excitation and e) mono-exponential decay on the order of tens to hundreds of microseconds with strongly temperature-dependent lifetimes (between −2.5 and −2.9% K^{-1} in polystyrene at 25 °C). Immobilization in gas-blocking polymers yields sensing materials for self-referenced decay time read-out that are manufactured in two common formats: planar optodes and water-dispersible nanoparticles. Positively charged nanoparticles are demonstrated to be suitable for nanothermometry in live cells and multicellular spheroids. Negatively charged nanoparticles represent advanced analytical tools for imaging temperature gradients in samples of small volumes such as microfluidic devices.

1. Introduction

Luminescent sensors are indispensable analytical tools that are distinguished by their high versatility of formats including planar foils, paints, fiber-optic sensors, and nanosensors. Nanosensors play an important role in understanding fundamental chemical processes in human and non-human cells and can help us to develop new drugs and therapies against diseases.[1–5] Among others, luminescent nanosensors have been reported for many important parameters such as pH,[6–8] oxygen,[9,10] ions,[11–13] and temperature.[14–16] Temperature is recognized as a fundamental parameter that can be altered by external and homeostatic causes.[17,18] Possible external causes include changes in ambient temperature or exposure to radiation.[19] Elevated cell temperatures have been measured, for example, in cancer cells and tissues[20–24] and during local inflammation in the affected cells.[25]

While classical thermometers such as resistance thermometers, thermocouples, and infrared thermometers are usually

A. Russegger, S. Fuchs, S. M. Borisov
Institute of Analytical Chemistry and Food Chemistry
Graz University of Technology
Stremayrgasse 9, Graz 8010, Austria
E-mail: sergey.borisov@tugraz.at

A. C. Debruyne, R. I. Dmitriev
Tissue Engineering and Biomaterials Group
Department of Human Structure and Repair
Faculty of Medical and Health Sciences
Ghent University
C. Heymanslaan 10, Ghent 9000, Belgium

The ORCID identification number(s) for the author(s) of this article can be found under https://doi.org/10.1002/adom.202202720.

DOI: 10.1002/adom.202202720

D. C. Berrio, J. Marzi, K. Schenke-Layland
Institute of Biomedical Engineering
Department for Medical Technologies and Regenerative Medicine and Cluster of Excellence iFIT (EXC 2180) "Image-Guided and Functionally Instructed Tumor Therapies"
Eberhard Karls University Tübingen
72076 Tübingen, Germany

J. Marzi, K. Schenke-Layland
NMI Natural and Medical Sciences Institute at the University of Tübingen
72770 Reutlingen, Germany

R. I. Dmitriev
Ghent Light Microscopy Core
Ghent University
Ghent 9000, Belgium

limited to a spatial resolution of 10 µm,[26] the spatial resolution of luminescent nanothermometers can go down to ≈200 nm with common confocal microscopes. Luminescent nanothermometers can be used in combination with fluorescence microscopes for generating 2D and 3D images of temperature gradients. For example, fluorescent polymeric thermometers were used to visualize the temperature distribution within COS-7 cells.[27] Here, an increased temperature in the nucleus and in the mitochondria compared to the cytoplasm was observed. In addition to temperature imaging in cells, nanothermometers can also be used in other areas where conventional temperature sensors fail due to their size, such as imaging in microfluidic chips,[28–31] micro flow reactors[32] and microfluidic devices for continuous-flow polymerase chain reaction (PCR).[33]

A large number of reported optical thermometers[34,35] can be divided into six readout groups depending on which luminescence property shows a temperature-dependent behavior: i) emission intensity, ii) spectral position of absorption and emission bands, iii) relative intensity between two emission bands, iv) emission bandwidth, v) anisotropy and vi) luminescence decay time.[36] Among these, measuring changes in a band shape and luminescence decay time are most popular due to robust read-out and self-referenced character.[26] Lifetime-based nanothermometers are particularly suitable for biological systems because this parameter is not affected by the dye concentration or by tissue scattering.[5] Intracellular lifetime-based temperature sensing has been realized with fluorescent dyes such as ER thermo yellow,[37] nanoparticle-embedded sulforhodamine derivative,[38] poly(*N*-isopropylamide) particles,[27,39,40] gold[41] and silver[42] nanoclusters and carbon dots.[43] Lifetime-based fluorescent and phosphorescent optical thermometers known outside of biological systems utilize ruthenium,[44] europium[45,46] and iridium[47] metal-organic complexes, inorganic phosphors,[48–50] silicon nanoparticles,[51] phase-change materials[52] and quantum dots.[53]

A great variety of emitters that utilize thermally activated delayed fluorescence (TADF) have been reported for application in organic light emitting diodes (OLEDs)[54,55] but only recently have they started drawing attention as components of sensing materials.[56] Earlier reports demonstrated potential of TADF emitters (acridine yellow,[57] fullerene C70[58,59]) for optical temperature sensing. More recently, several optical thermometers have been reported using organic dyes derived from anthraquinone and dicyanobenzene,[60] platinum(II), palladium(II), and zinc benzoporphyrins,[61,62] polymers based on 1,8-naphthalimide,[63] carbon dot-based nanocomposite[43] and zinc complexes with Schiff bases.[64,65] Although the luminescence decay was shown to be strongly affected by temperature at ambient conditions (>2% K^{-1}), practical usability of the state-of-the-art systems is still limited. The challenges include moderate luminescence brightness, significant contribution of prompt fluorescence to the overall emission, bi-exponential decay in immobilized form, and often very long TADF decay times (>1 ms) which imply significant cross-talk to molecular oxygen even in case of polymer matrices with low gas permeability.

Recently, Milsmann and coworkers reported a new class of TADF emitters based on readily synthetically available complexes of zirconium(IV) with substituted pyridinedipyrrolide (PDP) ligands.[66–68] Remarkably, the $Zr(PDP)_2$ complexes

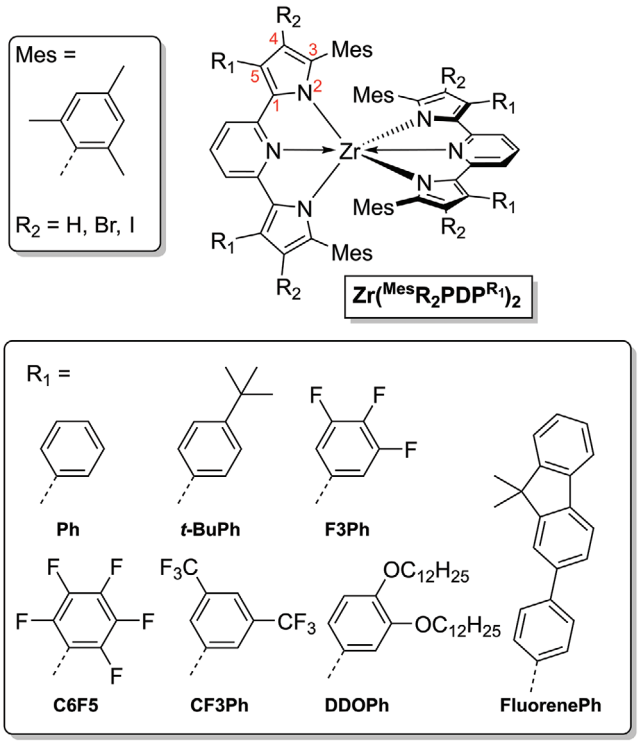

Figure 1. Structures of synthesized $Zr(PDP)_2$ complexes.

emit pure TADF emission without any prompt fluorescence and have TADF lifetimes of hundreds of microseconds. We perceived that this class of compounds is of highest relevance for lifetime-based optical (nano)thermometry and may help to overcome the disadvantages of state-of-the-art systems.

In this work, we report a series of zirconium(IV) pyridinedipyrrolide complexes (**Figure 1**) that combine attractive spectral properties, high brightness, and excellent photostability with highly temperature-dependent TADF decay time. The lifetimes can be tuned by varying the substituents on the PDP ligand and via straightforward introduction of "heavy" halogen atoms. The oxygen crosstalk can be almost completely avoided by embedding the complexes with the shortest lifetimes into gas-blocking polymers. Application of water-dispersible nanothermometers for imaging of temperature in microfluidic devices and biological systems is demonstrated.

2. Results and Discussion

2.1. Ligand Design and Synthesis of $Zr(PDP)_2$ Complexes

As became evident from the previous work,[60,65] TADF emitters of different dye classes are promising self-referenced molecular thermometers since they feature very high-temperature dependency on the emission decay time. For the envisaged applications such emitters should combine chemical stability with attractive spectral properties and high brightness of TADF. Moreover, it is desirable that the probes possess a relatively short TADF decay time (<1 ms and ideally <100 µs) in order to minimize cross-sensitivity to oxygen for polymer-immobilized dyes. Thus, we

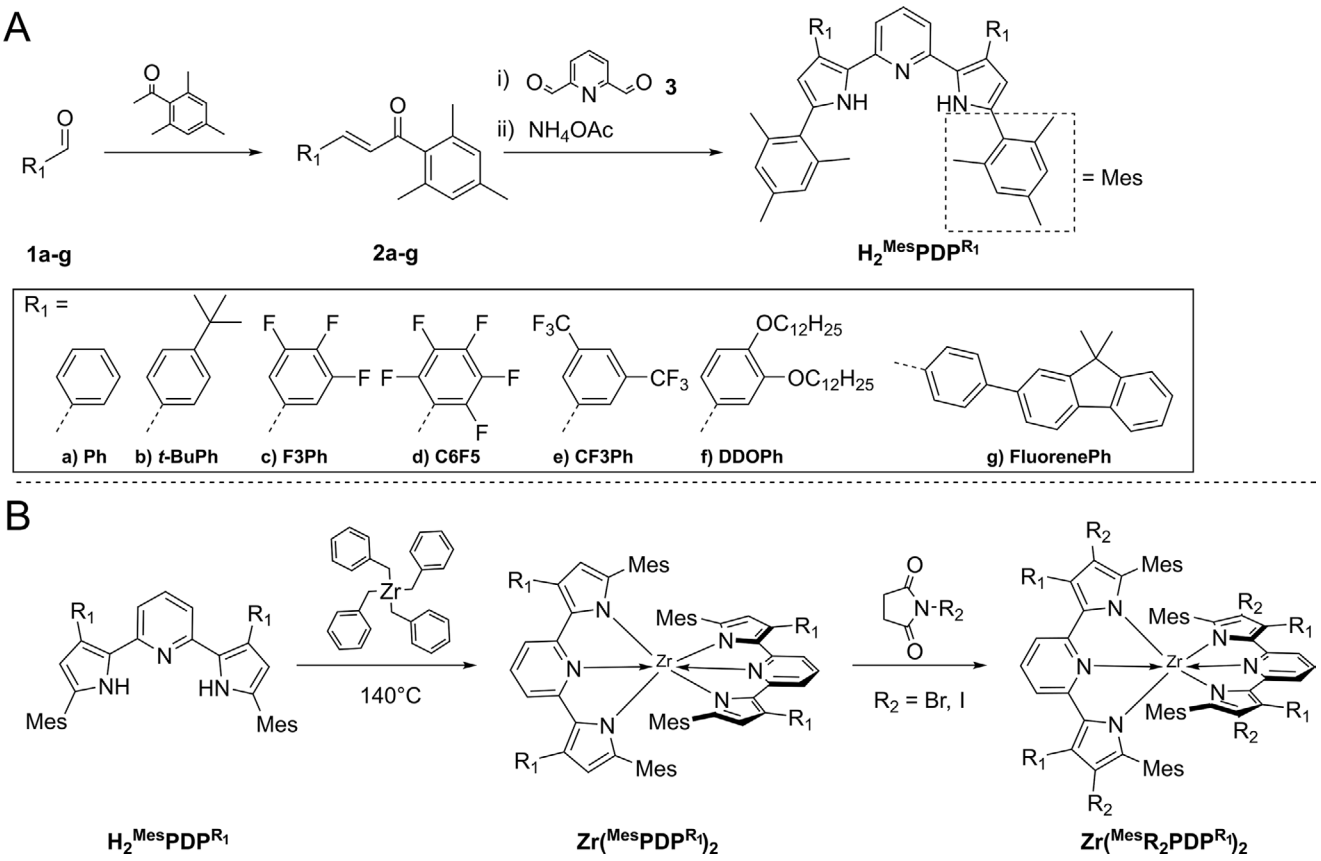

Scheme 1. A) Synthesis of $H_2{}^{Mes}PDP^{R}{}_1$-ligands and B) the $Zr(^{Mes}PDP^{R}{}_1)_2$ and $Zr(^{Mes}R_2PDP^{R}{}_1)_2$ complexes.

aimed at new hydrolytically stable $Zr(PDP)_2$ complexes with possibility of tuning the emission decay times. Substitution at the 3- and 5-positions of the PDP pyrrole rings (Figure 1) is known to have a significant effect on the photophysical properties and the stability of the complexes.[67] In fact, mesityl-groups (Mes) in the 3-positions were demonstrated to strongly enhance the hydrolytic stability making the $Zr(^{Mes}PDP^{Ph})_2$-complex stable under ambient conditions. On the other hand, substitution at the 5-position of the pyrrole rings can be used for fine-tuning the TADF lifetimes and quantum yields. For example, the compounds with an electron-withdrawing C_6F_5-group and an electron-donating methyl-group in the 5-positions were shown to have shorter (313 µs) and longer (576 µs) lifetimes, respectively, compared to the unsubstituted complex (τ_{TADF} = 474 µs).[67] The lifetimes of several hundred microseconds appear too long for applications as molecular thermometers since even embedded in gas-blocking polymers like polyacrylonitrile (PAN) and poly(vinylidene chloride-*co*-acrylonitrile) (PVDC-*co*-AN) these dyes would show some oxygen crosstalk.

Therefore, in order to tune the TADF decay times we combined two different strategies: i) introducing different electron-withdrawing and electron-donating groups at the 5-position of the PDP pyrrole rings and ii) additionally substituting the 4-position of the pyrroles with heavy atoms (bromine or iodine). Considering that the metal complex contains four pyrrole moieties, the latter modification was expected to be a viable strategy to significantly reduce the emission decay times. All the complexes were substituted with a mesityl-group at the 3-positions to ensure air and moisture stability. Overall, nine new $Zr(PDP)_2$ complexes were synthesized.

An overview of the dye synthesis is given in **Scheme 1**. In the first step, R_1-substituted aldehyde and 2′,4′,6′-trimethylacetophenone were condensed to the corresponding chalcone in aldol condensation. Then, the ligand $H_2{}^{Mes}PDP^{R}{}_1$ was formed in a two-step one-pot synthesis (Stetter and Paal-Knorr reactions) according to the reported protocol.[69] The reaction time of the second step (Paal-Knorr reaction) could be improved from >72 h to <8 h by refluxing the mixture in a synthesis reactor at 170 °C and a pressure of ≈20 bar. Next, $H_2{}^{Mes}PDP^{R}{}_1$ was complexed with tetrabenzylzirconium ($ZrBn_4$) to give $Zr(^{Mes}PDP^{R}{}_1)_2$ similar to literature.[68] Finally, in case of $Zr(^{Mes}PDP^{t\text{-}BuPh})_2$ and $Zr(^{Mes}PDP^{C6F5})_2$ the protons in the pyrrole rings were substituted with bromine/iodine using a corresponding succinimide derivative. Spectroscopic characterization of the complexes and intermediates by NMR-spectroscopy and mass spectroscopy (APCI-MS or MALDI-TOF) can be found in supporting information (Figures S19–S66 and Figures S67–S90 in Supporting Information, respectively).

2.2. Photophysical Properties

All complexes show spectral properties that are highly attractive for utilization in sensing (**Table 1**). They efficiently absorb

Table 1. Photophysical properties of $Zr(PDP)_2$ complexes in toluene at 25 °C.

Complex	$\lambda_{max,abs}$ (ε) [nm] ([M^{-1} cm^{-1}])	$\lambda_{max,em}$ [nm]	τ_{TADF} [µs]	$\Phi_{TADF\ rel.}$ [a] [a.u.]	$\Phi_{bl.}$ [µmol µmol^{-1}]
$Zr(^{Mes}PDP^{Ph})_2$	530 (20000)	595	282	0.46	4.9×10^{-7}
$Zr(^{Mes}PDPt^{\text{-}BuPh})_2$	530 (21700)	594	274	0.46	3.7×10^{-7}
$Zr(^{Mes}BrPDPt^{\text{-}BuPh})_2$	523 (18200)	593	147	0.48	1.4×10^{-7}
$Zr(^{Mes}IPDPt^{\text{-}BuPh})_2$	526 (20900)	593	127	0.47	4.4×10^{-9}
$Zr(^{Mes}PDP^{C6F5})_2$	519 (18000)	589	194	0.48	2.1×10^{-7}
$Zr(^{Mes}BrPD^{C6F5})_2$	522 (16300)	597	95.9	0.48	1.1×10^{-7}
$Zr(^{Mes}PDP^{F3Ph})_2$	529 (20400)	596	269	0.46	–
$Zr(^{Mes}PDP^{DDOPh})_2$	531 (23300)	595	270	0.46	–
$Zr(^{Mes}PDP^{CF3Ph})_2$	526 (21300)	589	253	0.48	–
$Zr(^{Mes}PDP^{FluorenePh})_2$	531 (25400)	600	213	0.46	–

[a] Relative to $Zr(^{Mes}PDP^{Ph})_2$ in THF ($\Phi = 0.45$).[68]

UV and blue-green parts of the electromagnetic spectrum and show orange emission (**Figure 2**). Substitution in the 5-position of the PDP pyrrole rings with electron-withdrawing or electron-donating groups only minimally affects the shape and position of absorption and emission bands (Figure 2; Figure S1, Supporting Information). Here, the stabilizing effects of the electron-withdrawing and slightly destabilizing effects of the electron-donating groups on the HOMO and HOMO+1 energies are almost completely compensated by an equivalent change in the LUMO and LUMO+1 energies, resulting in similar HOMO/LUMO energy gaps.[67] Substitution of hydrogen atoms in the 4-position of the pyrroles with bromine and iodine does not affect the spectral properties either. All the complexes are efficiently excitable with a variety of common LEDs (470, 505, or 525 nm) and Ar laser (488 and 514 nm lines).

The dyes feature one broad emission peak (full width at half maximum: ≈2300 cm^{-1}) in the orange to red part of the electromagnetic spectrum which on the basis of luminescence decays (**Figure 3**) is attributed purely to TADF emission. This property is remarkable since virtually all reported TADF emitters show prompt fluorescence in addition to TADF.[54,55] It should be noted that existence of prompt fluorescence on the cost of TADF would reduce the analytically useful signal in case of time-domain measurement and strongly reduce the phase resolution in frequency domain measurements.[70]

The quantum yields (Φ_{TADF}) of the complexes approach 50% and are very close to that of the parent compound $Zr(^{Mes}PDP^{Ph})_2$ (Φ = 0.46 in toluene, Table 1, and 0.45 in tetrahydrofuran[68]). The brightness ($\varepsilon \cdot \Phi$) is between 7800 and 10 200 M^{-1} cm^{-1} and is comparable to that of typical phosphorescent emitters such as platinum(II) meso-pentafluorophenyl porphyrin and ruthenium(II) tris-4,7-diphenyl-1,10-phenanthroline[71] and TADF emitters based on dicyanobenzene derivatives.[60]

Figure 3 and Figure S2 (Supporting Information) show that the luminescence of the dissolved dyes decays monoexponentially. In contrast to the extreme similarity in spectral properties, the TADF decay times (τ_{TADF}) are strongly affected by substitution in the 4- and 5-position of the pyrroles (Table 1). Substitution of the phenyl rings in the 5-positions with 4-*tert*-butylphenyl, 3,4,5-trifluorophenyl, and 3,4-didodecyloxyphenyl substituents result in very minor decrease of the decay time (<5%). Compared to $Zr(^{Mes}PDP^{Ph})_2$ the decay time decreases by ≈10% in case of 3,5-bis-trifluoromethyl substituents. The strongest effect is observed for pentafluorophenyl and 9,9-dimethylfluorene substituents: 31% and 24% decrease of the decay time for $Zr(^{Mes}PDP^{C6F5})_2$ and $Zr(^{Mes}PDP^{FluorenePh})_2$, respectively.

The introduction of heavy halogen atoms in the 4-position of the pyrroles results in a strong reduction of the TADF decay time. This is not unexpected, since heavy atoms promote more efficient intersystem crossing due to higher spin-orbit coupling[72] and the number of introduced heavy atoms is significant (four per molecule). In fact, the decay time decreases by 46% and 54% upon bromination and iodination, respectively, of $Zr(^{Mes}PDP^{t\text{-}BuPh})_2$. Similar decrease (51%) is observed upon bromination of $Zr(^{Mes}PDP^{C6F5})_2$ indicating that substitution effects in the 4- and 5-positions can be used independently for tuning the TADF decay time. $Zr(^{Mes}BrPDP^{C6F5})_2$ shows ≈3-fold lower lifetime compared to the reported $Zr(^{Mes}PDP^{Ph})_2$ (96 µs and 282 µs, respectively, at 25 °C) which is substantial considering that other photophysical properties are very similar.

Photostability of dyes is another important parameter, particularly in applications requiring relatively high light intensity such as microscopy. Evaluation of photostability was conducted for solutions of dyes in toluene that were irradiated by a metal-halide lamp. The decrease in the dye concentration was determined by UV–vis spectroscopy (Figure S3, Supporting Information). Tetramethylrhodamine ethyl ester perchlorate (TMR) dissolved in water was selected as a reference dye because it is generally considered as fairly photostable[73] and is frequently used as a fluorescence probe in microscopy.[74] The photobleaching quantum efficiencies (Φ_{bl}) were accessed for several selected dyes from the slope of the curves (amount of bleached dye vs amount of absorbed photons, **Figure 4**) and are summarized in Table 1. Remarkably, all dyes show better photostability than TMR ($\Phi_{bl} = 2.0 \times 10^{-6}$ µmol µmol^{-1}) (Figure 4). Although photostability of $Zr(^{Mes}PDP^{Ph})_2$ and $Zr(^{Mes}PDP^{t\text{-}BuPh})_2$ is 4-5-fold better than that of TMR, further

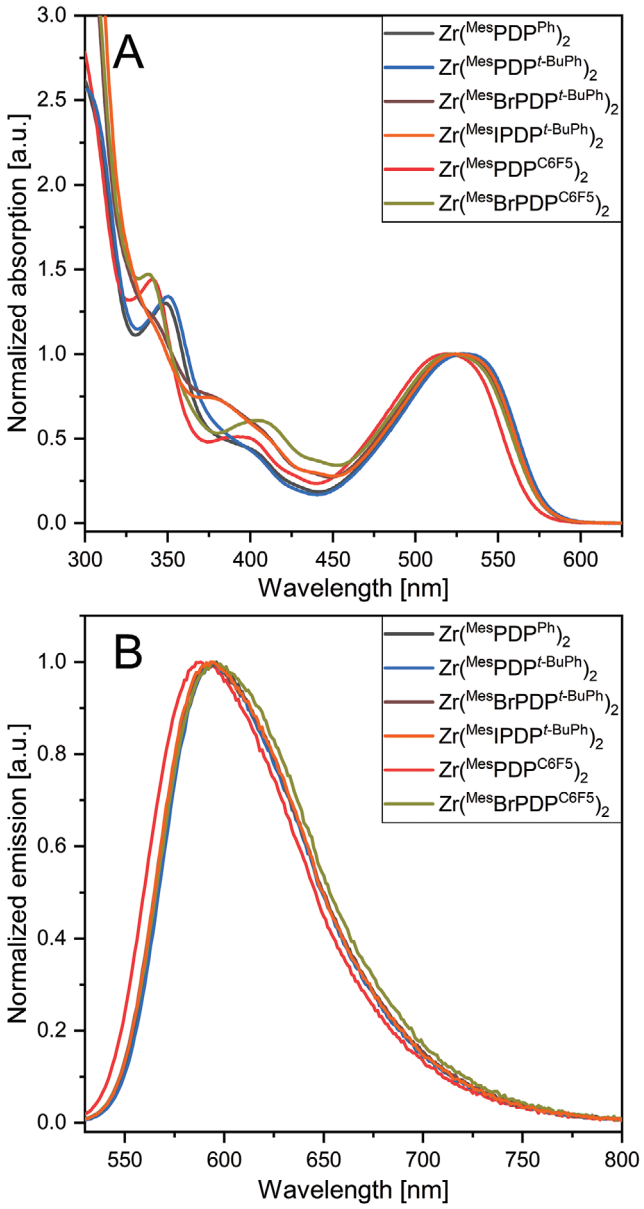

Figure 2. A) Absorption and B) emission spectra (λ_{exc} = 515 nm) of the $Zr(PDP)_2$ complexes measured in toluene at 25 °C. Emission spectra were measured under anoxic conditions.

improvement is evident for $Zr(^{Mes}PDP^{C6F5})_2$ and halogenated derivatives (Table 1). Substitution of phenyl groups in 5-position of pyrroles by pentafluorophenyl improves photostability by ≈2-fold (cf. $Zr(^{Mes}PDP^{Ph})_2$ and $Zr(^{Mes}PDP^{C6F5})_2$) and bromination has a similar effect (cf. $Zr(^{Mes}PDP^{t\text{-}BuPh})_2$ and $Zr(^{Mes}BrPDP^{t\text{-}BuPh})_2$; $Zr(^{Mes}PDP^{C6F5})_2$ and $Zr(^{Mes}BrPDP^{C6F5})_2$. Remarkable improvement of photostability is observed upon iodination in the 4-positions with $Zr(^{Mes}IPDP^{t\text{-}BuPh})_2$ showing ≈2-orders of magnitude slower bleaching than the parent $Zr(^{Mes}PDP^{Ph})_2$. In fact, it becomes challenging to reliably access such small photobleaching rates even using a high-power light source. Improvement of photostability upon substitution of phenyl groups by pentafluorophenyl in the 5-positions and

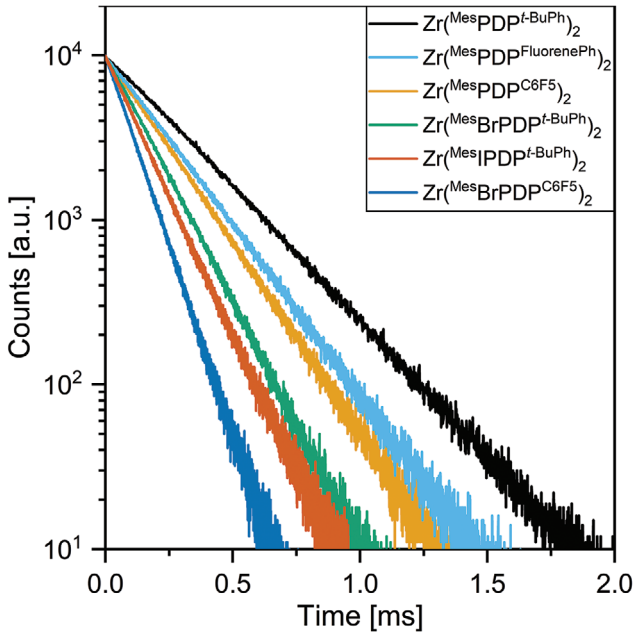

Figure 3. Mono-exponential luminescence decay of $Zr(PDP)_2$ complexes in toluene under anoxic conditions at 25 °C. The decays were recorded at the emission maxima of the dyes.

introduction of halogens in the 4-positions may be due to the combined effect of i) electron-withdrawing substituents that prevent oxidation of the chromophore by photosensitized singlet oxygen and ii) reduction in the lifetime of the triplet state that makes reactions involving significantly more reactive excited states less likely.

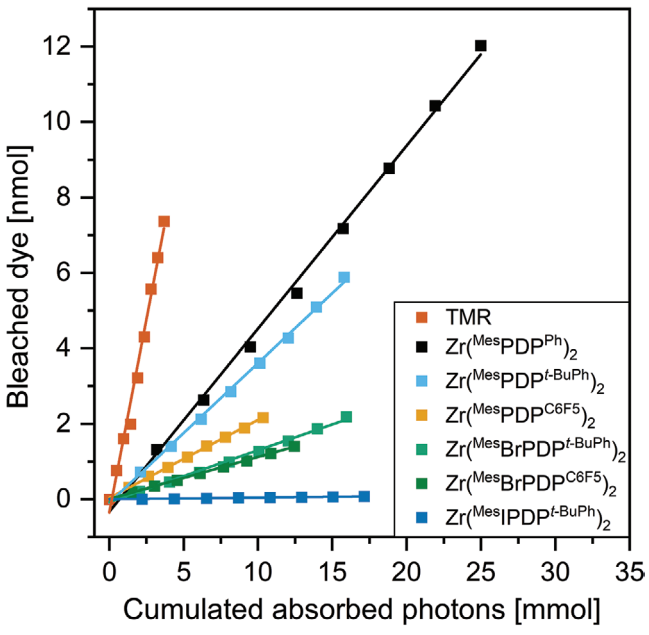

Figure 4. Photodegradation of $Zr(PDP)_2$ complexes (in toluene) and the reference TMR dye (in water) upon irradiation with metal-halide lamp (400–700 nm).

Table 2. Photophysical properties of $Zr(PDP)_2$ complexes in rigid polystyrene matrix under anoxic conditions at 25 °C.

Complex	$\lambda_{max,em}$ [nm]	τ_{TADF} (25 °C) [µs]	τ_{TADF} (37 °C)[a)] [µs]	$\Phi_{TADF\ abs.}$ [a.u.]	$d\tau/dT$ (25 °C) [% K^{-1}]
$Zr(^{Mes}PDP^{Ph})_2$	593	262	187	0.85 ± 0.03	−2.9
$Zr(^{Mes}PDPt^{-BuPh})_2$	591	253	182	0.84 ± 0.04	−2.9
$Zr(^{Mes}BrPDPt^{-BuPh})_2$	593	134	98.4	1.01 ± 0.05	−2.7
$Zr(^{Mes}IPDPt^{-BuPh})_2$	591	112	82.3	1.01 ± 0.05	−2.7
$Zr(^{Mes}PDP^{C6F5})_2$	594	172	125	0.91 ± 0.02	−2.8
$Zr(^{Mes}BrPDP^{C6F5})_2$	596	85.7	62.3	1.00 ± 0.04	−2.5
$Zr(^{Mes}PDP^{F3Ph})_2$	592	247	178	0.87 ± 0.05	−2.9
$Zr(^{Mes}PDP^{DDOPh})_2$	595	254	182	0.88 ± 0.02	−2.9
$Zr(^{Mes}PDP^{CF3Ph})_2$	587	232	167	0.94 ± 0.04	−2.9
$Zr(^{Mes}PDP^{FluorenePh})_2$	599	209	150	0.93 ± 0.02	−2.9

[a)]Lifetimes at 37 °C were obtained by interpolating the temperature calibration curves (Figure 5 and Figure S5, Supporting Information).

2.3. Evaluation of Temperature-Sensing Properties for Polystyrene-Immobilized Dyes

Temperature-sensing materials were prepared by immobilizing the dyes into polymer hosts. Polystyrene (PS) was used as a model substrate for evaluation of temperature-sensing properties of immobilized dyes. The dyes were dissolved in chloroform along with PS and the so-called "cocktails" were knife-coated on a transparent polyethylene terephthalate support. The materials were characterized under anoxic conditions, due to significant oxygen permeability of PS. The photophysical properties of these materials are summarized in **Table 2**.

Immobilization into a rigid matrix does not affect the emission spectra but leads to improvement of the TADF quantum yields that exceed 0.8. The three dyes with halogens in the 4-position of the pyrroles ($Zr(^{Mes}BrPDP^{t\text{-}BuPh})_2$, $Zr(^{Mes}IPDP^{t\text{-}BuPh})_2$, and $Zr(^{Mes}BrPDP^{C6F5})_2$) show the highest quantum yields of around unity.

All immobilized dyes show mono-exponential TADF decays (**Figure 5**A for $Zr(^{Mes}BrPDP^{C6F5})_2$ as an example) that are beneficial for sensing applications. This is in contrast to previously reported TADF emitters based on anthraquinones,[60] dicyanobenzenes,[60] and Zn(II) Schiff base complexes[64,65] which all showed bi- or tri-exponential decays in the immobilized form. Such behavior of the donor-acceptor dyes is attributed to existence of at least two different rotamers in the immobilized dyes since the rigid matrix prevents the dyes from rotation.[75] It is therefore likely that the zirconium complexes, which lack donor-acceptor character exist only in one form when immobilized into polymeric matrices.

The singlet-triplet energy gap ($\Delta E_{S1\text{-}T1}$) calculated from an Arrhenius plot for $Zr(^{Mes}PDP^{Ph})_2$ in PS (Figure S4, Supporting Information) is 1780 cm^{-1} which is similar to the value previously reported for $Zr(^{Mes}PDP^{Ph})_2$ in solution ($\Delta E_{S1\text{-}T1}$ = 1652 cm^{-1},[68] calculated from emission spectra).

Similar to other TADF emitters, the $Zr(PDP)_2$ complexes show high-temperature dependencies of their decay times (Figure 5B; Figure S5, Supporting Information). The sensitivity ($d\tau\, dT^{-1}$) at 25 °C is between −2.5 and −2.9% K^{-1} (Table 1) which exceeds the values shown by most state-of-the-art lifetime-based temperature sensing materials with the exception of TADF emitters.[65]

In contrast to the high-temperature dependency on the TADF lifetimes, the emission intensities of the embedded dyes remain almost constant (<5% variation) in the temperature range between 10 °C and 50 °C (**Figure 6**; Figure S6, Supporting Information). This implies very stable signals and signal-to-noise ratios over a wide temperature range. Generally, TADF emitters show strong enhancement of delayed fluorescence with temperature[76,77] which is also the case for the zirconium pyridinedipyrrolide complexes, albeit in sub-zero temperature range.[68] At ambient conditions, the emission is thus fully "activated". In comparison, most of the reported optical thermometers including phosphorescent and fluorescent dyes and inorganic phosphors show a strong decrease in emission intensity with increasing temperature due to enhancement in the radiationless deactivation ("thermal quenching"). This typical behavior is exemplified in Figure 6 for an Eu(III) complex ($Eu(tta)_3DEADIT$)[78] immobilized in PS. In fact, the luminescence intensity decreases ≈3-fold on going from 10 °C to 50 °C.

2.4. Planar and Fiber-Optic Temperature Sensors

Sensing materials based on PS cannot be used for temperature measurements under aerated conditions due to the significant oxygen permeability of PS (1.9×10^{-13} cm^3 (STP) cm cm^{-2} s^{-1} Pa^{-1}[79]). To overcome this problem, $Zr(^{Mes}BrPDP^{C6F5})_2$, the dye with the shortest lifetime among all investigated complexes, was immobilized into PVDC-*co*-AN. The combination of the very low oxygen permeability of PVDC-*co*-AN (0.0031×10^{-13} cm^3 (STP) cm cm^{-2} s^{-1} Pa^{-1}[80]) and the short lifetimes of $Zr(^{Mes}BrPDP^{C6F5})_2$ drastically reduces the cross-talk to oxygen. In fact, the luminescence lifetimes in temperature range between 10 °C and 50 °C decrease by < 2% on going from deoxygenated to air-saturated water (**Figure 7**). Without knowing the exact oxygen concentration, this corresponds to the maximum

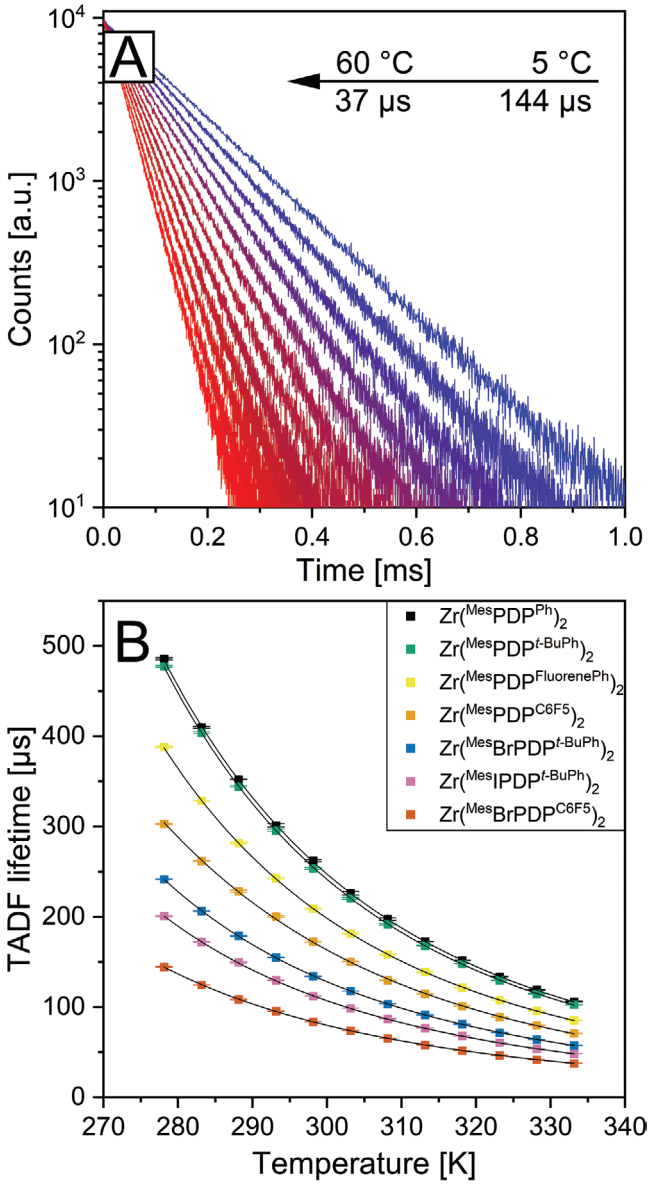

Figure 5. A) Mono-exponential luminescence decays of $Zr(^{Mes}BrPDP^{C6F5})_2$ in PS between 5 °C and 60 °C (5 °C steps) under anoxic conditions. The decays were recorded at the emission maximum of 596 nm. B) Temperature dependency of TADF decay times for $Zr(PDP)_2$ complexes immobilized in PS acquired under anoxic conditions. For the temperature dependency measurements, three calibration cycles were performed.

error of ≈0.4 °C between air-saturated and deoxygenated conditions. However, in many applications, the oxygen concentration remains nearly constant so that the error can be neglected.

The same material was used to prepare a fiber-optic sensor. A layer of $Zr(^{Mes}BrPDP^{C6F5})_2$-PVDC-*co*-AN on polyethylene terephthalate support was coated with an additional scattering layer (titanium dioxide particles in silicone rubber) to achieve higher signals when read-out with a custom version of a compact phase fluorometer (Firesting, PyroScience) that was equipped with a blue LED (465 nm) for excitation. A sensor spot prepared from a planar foil and fixed with a metal cap on an optical fiber

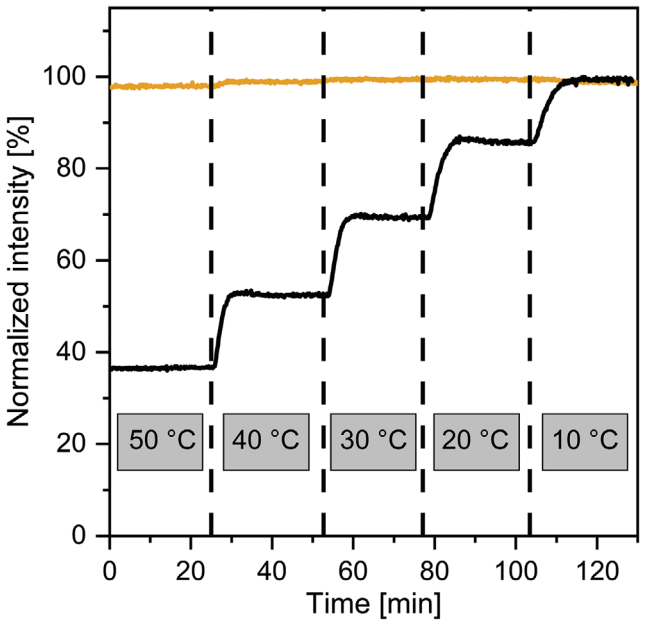

Figure 6. Temperature dependency of emission intensity for $Zr(^{Mes}IPDP^{t\text{-}BuPh})_2$ (orange line) and $Eu(tta)_3$DEADIT (black line) immobilized in PS, recorded between 10 °C and 50 °C under anoxic conditions. The dyes were excited at the lowest-energy absorption maxima (530 and 413 nm, respectively) and their emission intensity was measured at the emission maximum (593 and 615 nm, respectively).

operated fully reversibly (Figure S7, Supporting Information). Possible applications of such a sensor include measurements of temperature in strong magnetic fields or local measurements in small objects like microfluidic chips.[28–30]

2.5. Water-Dispersible Nanoparticles

Immobilization of the zirconium complexes in nanoparticles based on oxygen-blocking polymers would enable "nanothermometry", i.e., temperature measurement in small objects such as live cells, tissues, and microfluidic chips. Since nanoparticles prepared from PVDC-*co*-AN are rather large and lack stability, particularly in the presence of salts, the polymer was modified with charged groups to ensure stability in aqueous dispersion and to enable cell interactivity. For this purpose, the gas-blocking PVDC-*co*-AN polymer was modified to additionally incorporate either ≈10 wt.% methacrylic acid (MAA) or ≈10 wt.% [2-(methacryloyloxy)-ethyl]-trimethylammonium chloride (TMA). This leads to negatively- and positively-charged copolymers, abbreviated as PVA-MAA and PVA-TMA, respectively. Nanoprecipitation technique[81] offers a simple way to obtain dye-loaded polymeric nanoparticles. Fast addition of water to the solution of a copolymer and a dye in acetone or its mixtures with other solvents and subsequent removing of the organic solvents via evaporation gives particles of 34 nm (PVA-MAA, zeta potential: -16 mV) and 42 nm (PVA-TMA, zeta potential: +35 mV) (Figures S8 and S9, Supporting Information). We note that in the second case, the size distribution is not homogenous, and significantly larger particles are also

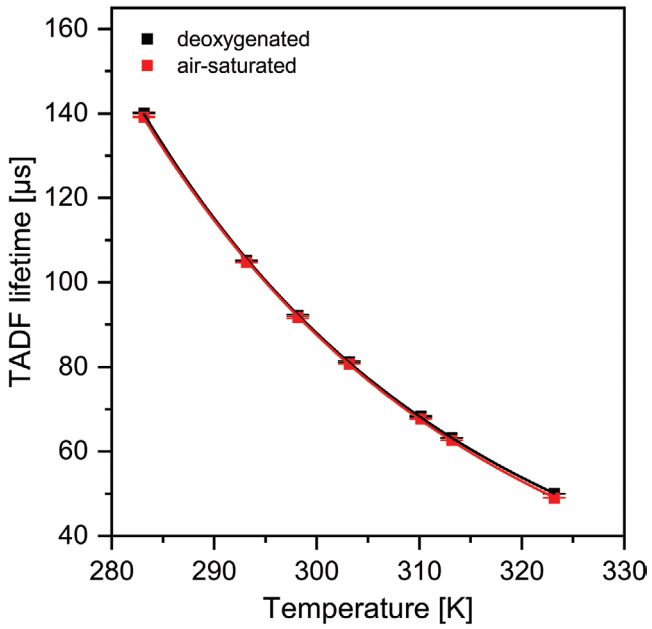

Figure 7. Temperature dependency of TADF decay times (measured via time correlated single photon counting, TCSPC) for $Zr(^{Mes}BrPDP^{C6F5})_2$ immobilized in PVDC-*co*-AN acquired in deoxygenated and air-saturated water.

present, which can require the need for further optimization of the polymer composition and nanoprecipitation procedure.

In order to show the potential of the new tools for imaging of temperature distribution, we incorporated $Zr(^{Mes}IPDP^{t\text{-}BuPh})_2$ into negatively charged cell-impermeable PVA-MAA nanoparticles and applied them for in-chip imaging. $Zr(^{Mes}IPDP^{t\text{-}BuPh})_2$ and $Zr(^{Mes}BrPDP^{C6F5})_2$ were embedded into positively charged PVA-TMA nanoparticles for intracellular imaging.

In the first application, a $Zr(^{Mes}IPDP^{t\text{-}BuPh})_2$-PVA-MAA particle suspension (≈22 °C) was pumped at different flow rates (between 0 and 10 µL s^{-1}) through a microfluidic chip which was heated to ≈37 °C. The temperature distribution was imaged with a frequency domain fluorescence lifetime imaging (FLIM) camera from PCO Computer Optics (**Figure 8**).

Figure 8 demonstrates that at low flow rates (1-2 µL s^{-1}), the colder nanoparticles solution quickly achieved the set temperature within the chip. At higher flow rates, constant temperature in the chip was no longer uniformly sustained and drastic gradients of >10 °C were observed. Considering the growing importance of temperature for cell metabolism studies and as a parameter affecting analytical response of every optical sensor, these new materials can be applied to many tissue-on-a-chip experimental platforms.

In the second application, we evaluated applicability of the positively charged nanoparticles for the live cell nanothermometry. First, we looked at the effect of the nanoparticle surface charge (PVA-MAA and PVA-TMA particles) on the interaction with the cells (Figure S11, Supporting Information). As expected, negatively charged nanoparticles displayed much lower staining of the human colon cancer HCT116, endothelial HUVEC, and dental pulp stem cells. In contrast, quaternary ammonium groups harboring $Zr(^{Mes}IPDP^{t\text{-}BuPh})_2$-PVA-TMA nanoparticles promoted efficient endo- and lysosome-like staining (**Figure 9**A–C; Figure S12, Supporting Information), similar to other previously described nanosensors.[9,12,38,82] As with the sulforhodamine-based temperature probe,[38] we saw no effect of the positively charged nanoparticles on the cell viability (Figure S13, Supporting Information). We also observed relatively long retention of the nanoparticles inside the cells, lasting longer than 48 h (Figure S14, Supporting Information). These features prompted us to see if we could also measure temperature in more complex cell-based models, such as multicellular 3D spheroids produced from HCT116 cells (Figure 9D–F; Figure S15, Supporting Information).

Despite somehow patchy distribution in the spheroids, we managed to measure the emission lifetimes (≈49 µs) at the periphery of the live spheroids using a 485 nm excitation and confocal microscope (Figure 9E,F).

To improve the imaging quality and expand the scope of potential biological applications with spheroids, related organoid models, or intravital measurements, two-photon (2P) excitation can be used alternatively.[1,83] We thus tested the compatibility of $Zr(^{Mes}IPDP^{t\text{-}BuPh})_2$ embedded into PVDC-*co*-AN with the 2P excitation. The material was compared to Rhodamine B immobilized in the same polymer. The latter was

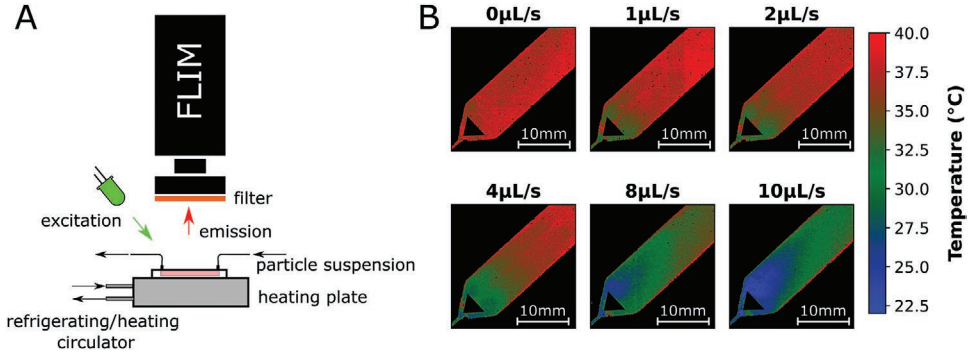

Figure 8. Imaging of temperature distribution in a microfluidic chip with an aqueous dispersion of $Zr(^{Mes}IPDP^{t\text{-}BuPh})_2$-PVA-MAA nanoparticles. A) Experimental setup; B) temperature distribution in a heated microfluidic chip (≈37 °C) through which a colder particle suspension (≈22 °C) was pumped at a flow rate between 0 and 10 µL s^{-1}. The pictures were recorded after 1 min at the corresponding flow rate.

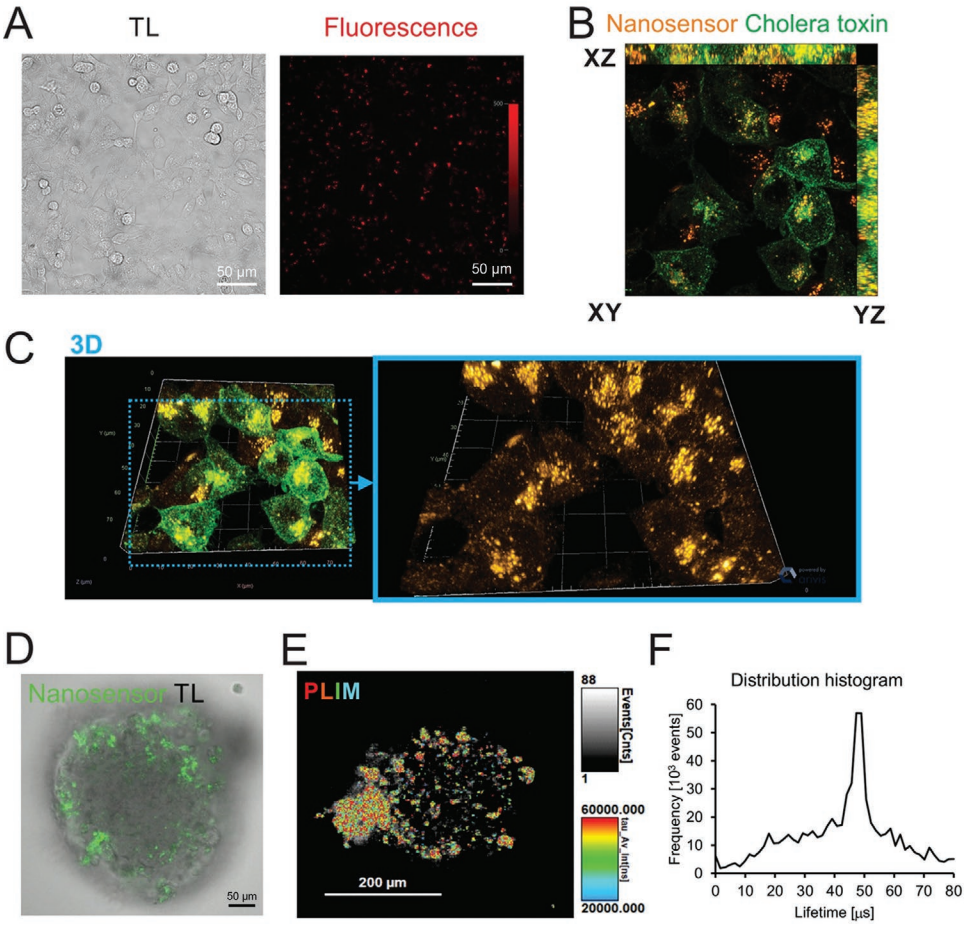

Figure 9. Evaluation of Zr(^{Mes}IPDP$^{t\text{-}BuPh}$)$_2$-PVA-TMA nanoparticles with HCT116 cells. A) Staining of live HCT116 cells with nanoparticles (5 µg mL^{-1}, 17 h). Transmission light (TL) and fluorescence (red) are shown. B,C) 3D reconstruction of nanoparticles localization inside HCT116 cells, co-stained with cholera toxin-Alexa Fluor 488. Cells were stained with nanoparticles (5 µg mL^{-1}, 17 h) and cholera toxin (2 µM, 1 h), washed, fixed with paraformaldehyde, and analyzed by 3D confocal microscopy. B) shows ortho slices (maximum intensity projection). Image size: 78.21 × 78.21 µm, Z stack of 41 slices (6.8 µm). C) 3D projections of stained cells at various magnifications. Right panel shows nanosensor (orange) distribution without cholera toxin counter stain. D) Confocal microscopy of live spheroid stained with 5 µg mL^{-1} nanoparticle (combined transmission light and fluorescence images, excited at 488 nm). E,F) Phosphorescence lifetime imaging (PLIM) of live multicellular spheroid using confocal microscopy (λ_{exc} = 485 nm). E) Combined intensity and PLIM images. Grayscale and colormap on the right indicate intensity counts and average lifetime in ns (20 000 to 60 000 ns, from blue to red). F) Luminescence lifetime distribution histogram.

selected as a standard since its emission spectrum is similar to that of the Zr(^{Mes}IPDP$^{t\text{-}BuPh}$)$_2$ complex. Rhodamine B is reported to show two-photon absorption (2PA) maximum at ≈820–840 nm with the estimated 2PA cross-sections between 200 GM[84,85] and 500 GM.[86] Figure S16 (Supporting Information) shows that both dyes are excitable in approximately the same part of the spectrum. Zr(^{Mes}IPDP$^{t\text{-}BuPh}$)$_2$ shows rather a broad excitation which is most efficient from 710 to 810 nm. Emission spectra (Figure S17, Supporting Information) show much higher luminescence intensity in case of the reference dye obtained for the same concentrations, excitation wavelength (800 nm), and laser power. In fact, except for the lowest concentration of 0.5 µmol g^{-1} polymer the signal from Rhodamine B was too high at the excitation power of 5% (Figure S17B, Supporting Information). Considering that the emission quantum yields of both dyes are quite similar, the 2PA cross-section for Zr(^{Mes}IPDP$^{t\text{-}BuPh}$)$_2$ is estimated to be ≈25-fold lower than for Rhodamine B, i.e., in the range of 10–20 GM. Nevertheless, these values are generally sufficient for 2P microscopy and are higher than for many dyes bearing no additional 2P antennas.[87] Indeed, we found that nanoparticle-stained multicellular spheroids were sufficiently bright for measurements by 2P phosphorescence lifetime imaging microscopy (Figure S15, Supporting Information).

We also investigated the non-linear properties of Zr(^{Mes}PDP^{FluorenePh})$_2$ to see if the fluorene moiety can serve as a 2P antenna. Indeed, the 2P excitation spectrum of this dye is different from Zr(^{Mes}IPDP$^{t\text{-}BuPh}$)$_2$ (Figure S18, Supporting Information). Much broader excitation band and maximum at ≈700 nm indicate that under 2P both the chromophore and the fluorene antenna can be excited. However, the 2PA cross-sections are estimated to be lower than for Zr(^{Mes}IPDP$^{t\text{-}BuPh}$)$_2$, so such modification appears not to lead to improvement of the non-linear properties.

3. Conclusion

In summary, we have synthesized and characterized a series of nine substituted zirconium(IV) pyridinedipyrrolide complexes bearing various electron-donating and electron-withdrawing groups in the 4- and 5-position of the PDP pyrrole rings. The complexes can be excited in the blue and green regions of the electromagnetic spectrum, are highly photostable, and show excellent brightness under one-photon excitation and acceptable characteristics under two-photon excitation mode. Moreover, the dyes show a unique combination of photophysical properties that are particularly attractive for optical temperature sensing applications: i) pure TADF emission without prompt fluorescence; ii) mono-exponential luminescence decay; iii) high-temperature dependency of the TADF decay time between –2.5 and –2.9% change per K at 25 °C; and iv) virtually constant TADF intensity in the relevant temperature range.

The introduction of a strongly electron-withdrawing C_6F_5-group in the 5-positions and heavy atoms (Br and I) in the 4-positions, led to a drastic reduction in the TADF lifetime (up to ≈3-fold) compared to the previously reported $Zr(^{Mes}PDP^{Ph})_2$ complex. Such substitution is beneficial for temperature sensing applications since it significantly reduces potential cross-talk with oxygen but has almost no effect on other photophysical properties. Additionally, it was found that heavy atoms could further enhance photostability which can be beneficial for other photonics applications such as OLEDs and photocatalysis.

Immobilization of the new probes into gas-blocking copolymer of vinylidene chloride and acrylonitrile gives materials for temperature sensing and imaging, that can be realized in a variety of formats such as planar foils, fiber-optic sensors, and water-dispersible nanoparticles. The latter can harbor anionic or cationic functional groups to ensure stability in water and addressable character in biological applications. We demonstrated application of nanoparticles in imaging of temperature gradients within a microfluidic chip and in cellular imaging. We found the positively charged nanoparticles compatible with the lifetime-based nanothermometry of 3D cultures of the live cells. Collectively, presented materials can be useful for a broad range of biological applications, complementing studies of cell metabolism, senescence, and development, under static and fluidic flow conditions.

4. Experimental Section

Materials: Benzaldehyde (1a), 3,4,5-trifluorobenzaldehyde (1c), 2,3,4,5,6-pentafluorobenzaldehyde (1d), and tetrabenzylzirconium(IV) were purchased from ABCR, [2-(methacryloyloxy)ethyl] trimethylammonium chloride (80 wt.% in H_2O), 1,1-dichloroethene, acrylonitrile, D-(+)-glucose monohydrate, glucose oxidase from *A. niger* (≈200 U mg^{-1}), methacrylic acid, sodium *tert*-butoxide, tetramethylrhodamine ethyl ester perchlorate, Rhodamine B and titanium(IV) chloride tetrahydrofuran complex ($TiCl_4(THF)_2$) were obtained from Sigma Aldrich, dichloromethane (DCM) and ethanol (EtOH) were from Fisher Scientific. 4-*tert*-Butylbenzaldehyde (1b), hexafluoro-2-propanol, *N*-bromosuccinimide (NBS) and *N*-iodosuccinimide (NIS) were purchased from TCI Europe. 1,2,4-Trimethylbenzene and 2′,4′,6′-trimethylacetophenone were from Alfa Aesar, 3,5-bis(trifluoromethyl)benzaldehyde (1e), 3-benzyl-5-(2-hydroxyethyl)-4-methylthiazolium chloride were obtained from Fluorochem. Azobisisobutyronitrile (AIBN) and polystyrene (PS, average M.W. 260 000 Da) were from Acros Organics. Ammonium acetate (NH_4OAc), anhydrous sodium sulfate (Na_2SO_4), chloroform, sodium sulfite (Na_2SO_3), triethylamine, and toluene (HPLC grade) were purchased from Carl Roth. Deuterated solvents were obtained from Eurisotop. Acetone, cyclohexane (CH), ethyl acetate (EA), heptane, hydrochloric acid 37%, sodium hydroxide (NaOH), and tetrahydrofuran (THF) were from VWR Chemicals. Silica gel 60 (0.063–0.200 mm), sodium chloride, heptane, and *tert*-butyl alcohol were purchased from Merck. Poly(ethylene terephthalate) (PET) support was received from Pütz. Ultrafine titanium dioxide (TiO_2) powder (UV-TITAN P170) was from Kemira. Silicone E4 was purchased from Wacker chemicals. Poly(vinylidene chloride-*co*-acrylonitrile (PVDC-*co*-AN, average M.W. 125 000 Da, acrylonitrile content: 20 wt.%) was obtained from Scientific Polymer Products, Inc.

Synthesis: 3,4-Bis-dodecyloxy-benzaldehyde[88] (1f), 4-(9,9-dimethyl-9H-fluoren-2-yl)benzaldehyde[89] (1g), and pyridine-2,6-dicarbaldehyde[90] (3) were synthesized according to literature. Flash chromatography was performed by a Biotage Select system using Sfär Silica columns from Biotage. A Monowave 50 synthesis reactor from Anton Paar was used for performing reactions under high pressure.

Synthesis of 1-mesityl-3-phenylprop-2-en-1-one (2a): NaOH (330 mg, 8.25 mmol, 1.3 eq) was dissolved in a mixture of H_2O (3 mL) and EtOH (1.5 mL) and 2′,4′,6′-trimethylacetophenone (1.00 g, 6.16 mmol, 1 eq) was added. After 15 min, benzaldehyde (1a) (720 mg, 6.78 mmol, 1.1 eq) was added dropwise and the solution was stirred overnight at room temperature. Afterward, the yellow mixture was extracted three times with DCM, the organic layer was dried over Na_2SO_4 and the solvent was removed under reduced pressure. The crude product was purified by column chromatography (silica gel) using a gradient from CH to CH:EA (9:1 v/v) as an eluent and was isolated as a yellow oil. Yield: 1.29 g (84%).

^{1}H NMR (300 MHz, $CDCl_3$) δ = 7.55 – 7.47 (m, 2H), 7.44 – 7.34 (m, 3H), 7.19 (d, J = 16.3, 1H), 6.99 – 6.84 (m, 3H), 2.33 (s, 3H), 2.19 (s, 6H). ^{13}C NMR (76 MHz, $CDCl_3$) δ = 201.51, 146.78, 138.52, 137.26, 134.62, 134.24, 130.91, 129.10, 128.61, 128.52, 21.28, 19.47.

APCI-MS *m/z*: calc. for $C_{18}H_{19}O$ $[M + H]^+$: 251.1, found: 251.1.

Synthesis of 3-(4-(tert-butyl)phenyl)-1-mesitylprop-2-en-1-one (2b): NaOH (130 mg, 3.25 mmol, 1.3 eq) was dissolved in a mixture of H_2O (0.5 mL) and EtOH (1.5 mL) and 2′,4′,6′-trimethylacetophenone (400 mg, 2.77 mmol, 1 eq) was added. After 15 min, 4-*tert*-butylbenzaldehyde (1b) (450 mg, 2.77 mmol, 1.1 eq) was added dropwise and the solution was stirred overnight at 50 °C. Afterward, the yellow mixture was extracted three times with DCM, the organic layer was dried over Na_2SO_4 and the solvent was removed under reduced pressure. The crude product was purified by flash chromatography using a gradient from CH to CH:DCM (1:1 v/v) as an eluent and was isolated as a yellow oil. Yield: 470 mg (62%).

^{1}H NMR (300 MHz, CD_2Cl_2) δ = 7.52 – 7.36 (m, 4H), 7.14 (d, J = 16.2, 1H), 6.97 – 6.81 (m, 3H), 2.33 (s, 3H), 2.16 (s, 6H), 1.32 (s, 9H). ^{13}C NMR (76 MHz, CD_2Cl_2) δ = 201.50, 155.09, 146.98, 138.84, 137.96, 134.59, 132.40, 128.82, 128.35, 126.52, 35.41, 31.42, 21.43, 19.61.

APCI-MS *m/z*: calc. for $C_{22}H_{27}O$ $[M + H]^+$: 307.2, found: 307.3.

Synthesis of 1-mesityl-3-(3,4,5-trifluorophenyl)prop-2-en-1-one (2c): NaOH (35 mg, 875 µmol, 1.4 eq) was dissolved in a mixture of H_2O (1.5 mL) and EtOH (1 mL) and 2′,4′,6′-trimethylacetophenone (100 mg, 616 µmol, 1 eq) was added. After 15 min, 3,4,5-trifluorobenzaldehyde (1c) (103 mg, 643 µmol, 1 eq) was added dropwise and the solution was stirred overnight at room temperature. Afterward, the yellow mixture was extracted three times with DCM, the organic layer was dried over Na_2SO_4 and the solvent was removed under reduced pressure. The crude product was purified by flash chromatography using a gradient from CH to CH:DCM (1:1 v/v) as an eluent and was isolated as a yellow oil. Yield: 110 mg (57%).

^{1}H NMR (300 MHz, CD_2Cl_2) δ = 7.17 (dd, J = 8.3, 6.4, 2H), 7.03 (d, J = 16.2, 1H), 6.90 (s, 2H), 6.81 (d, J = 16.2, 1H), 2.32 (s, 3H), 2.16 (s, 6H). ^{13}C NMR (76 MHz, CD_2Cl_2) δ = 200.62, 153.68, 150.36, 143.08, 143.04, 139.69, 139.36, 137.35, 134.63, 131.63, 130.99, 128.99, 112.94, 21.42, 19.63.

APCI-MS *m/z*: calc. for $C_{18}H_{16}F_3O$ $[M + H]^+$: 305.1, found: 305.1.

Synthesis of 1-mesityl-3-(perfluorophenyl)prop-2-en-1-one (2d): In a flame-dried Schlenk tube, 2′,4′,6′-trimethylacetophenone (167 mg, 1.30 mmol, 1 eq) was dissolved in dry DCM (2 mL) under an argon atmosphere. Dry triethylamine (115 mg, 1.14 mmol, 1 eq) and $TiCl_4(THF)_2$ (339 mg, 1.00 mmol, 1 eq) were added in one portion and the reaction was stirred for 15 min at room temperature. In a second flame-dried Schlenk tube 2,3,4,5,6-pentafluorobenzaldehyde (1d) (217 mg, 1.11 mmol, 1 eq) and $TiCl_4(THF)_2$ (340 mg, 1.00 mmol, 1 eq) were dissolved in dry DCM (1 mL). The solution containing the ketone was added portion-wise to the aldehyde solution. The reaction was stirred for 60 min at room temperature. Afterward, HCl (2 mL, 1 mol L^{-1}) was added and the product was extracted twice with DCM. The organic layer was washed twice with brine, dried over Na_2SO_4 and the solvent was removed under reduced pressure. The crude product was purified by flash chromatography using a gradient from CH to CH:EA (5:1 v/v) as an eluent and was isolated as a yellow solid. Yield: 301 mg (80%).

^{1}H NMR (300 MHz, CD_2Cl_2) δ = 7.21 (d, J = 16.7, 1H), 7.14 (d, J = 17.1, 1H), 6.91 (s, 2H), 2.32 (s, 3H), 2.18 (s, 6H). ^{13}C NMR (76 MHz, CD_2Cl_2) δ = 200.47, 147.82, 146.26, 144.46, 140.69, 140.11, 139.71, 136.91, 136.77, 135.86, 134.77, 129.35, 129.11, 21.44, 19.72.

APCI-MS m/z: calc. for $C_{18}H_{14}F_5O$ $[M + H]^+$: 341.1, found: 341.0.

Synthesis of 3-(3,5-bis(trifluoromethyl)phenyl)-1-mesitylprop-2-en-1-one (2e): NaOH (80 mg, 2.00 mmol, 1.3 eq) was dissolved in a mixture of H_2O (0.5 mL) and EtOH (1 mL) and 2′,4′,6′-trimethylacetophenone (250 mg, 1.54 mmol, 1 eq) was added. After 15 min, 3,5-bis(trifluoromethyl) benzaldehyde (1e) (373 mg, 1.54 mmol, 1 eq) was added dropwise and the solution was stirred for 2 h at room temperature. Afterward, the yellow mixture was extracted three times with DCM, the organic layer was dried over Na_2SO_4 and the solvent was removed under reduced pressure. The crude product was purified by flash chromatography using a gradient from CH to CH:DCM (7:3 v/v) as an eluent and was isolated as a yellow oil. Yield: 385 mg (64%).

^{1}H NMR (300 MHz, CD_2Cl_2) δ 7.97 (s, 2H), 7.91 (s, 1H), 7.21 (d, J = 16.3 Hz, 1H), 7.02 (d, J = 16.3 Hz, 1H), 6.92 (s, 2H), 2.33 (s, 3H), 2.17 (s, 6H). ^{13}C NMR (76 MHz, CD_2Cl_2) δ 200.72, 142.74, 139.51, 137.47, 137.15, 134.67, 133.44, 133.00, 132.55, 132.18, 129.04, 128.68, 125.51, 124.16, 121.90.

APCI-MS m/z: calc. for $C_{20}H_{17}F_6O$ $[M + H]^+$: 387.1, found: 386.7.

Synthesis of 3-(3,4-bis(dodecyloxy)phenyl)-1-mesitylprop-2-en-1-one (2f): NaOH (26 mg, 650 µmol, 1.3 eq) was dissolved in a mixture of H_2O (0.5 mL) and EtOH (1.5 mL) and 2′,4′,6′-trimethylacetophenone (800 mg, 493 µmol, 1 eq) was added. After 15 min, 3,4-bis-dodecyloxy-benzaldehyde (1f) (250 mg, 526 µmol, 1.1 eq) was added dropwise and the solution was stirred overnight at 60 °C. Afterward, the yellow mixture was extracted three times with DCM, the organic layer was dried over Na_2SO_4 and the solvent was removed under reduced pressure. The crude product was purified by flash chromatography using a gradient from CH to CH:DCM (1:1 v/v) as an eluent and was isolated as a yellow solid. Yield: 224 mg (73%).

^{1}H NMR (300 MHz, CD_2Cl_2) δ 7.17 – 6.98 (m, 3H), 6.98 – 6.70 (m, 4H), 3.99 (q, J = 6.8 Hz, 4H), 2.32 (s, 3H), 2.16 (s, 6H), 1.79 (p, J = 6.6 Hz, 4H), 1.46 (t, J = 7.4 Hz, 4H), 1.28 (s, 32H), 0.88 (t, J = 6.5 Hz, 6H). ^{13}C NMR (76 MHz, CD_2Cl_2) δ = 201.28, 152.45, 149.88, 147.33, 138.71, 138.17, 134.57, 128.78, 127.87, 126.89, 123.67, 113.49, 112.99, 69.88, 69.65, 32.53, 30.29, 30.26, 30.23, 29.97, 29.87, 29.76, 26.61, 26.58, 23.29, 21.43, 19.62, 14.47.

APCI-MS m/z: calc. for $C_{42}H_{67}O_3$ $[M + H]^+$: 619.5, found: 619.4.

Synthesis of 3-(4-(9,9-dimethyl-9H-fluoren-2-yl)phenyl)-1-mesitylprop-2-en-1-one (2g): NaOH (43 mg, 1.07 mmol, 1.3 eq) was dissolved in a mixture of H_2O (1 mL) and EtOH (2 mL) and 2′,4′,6′-trimethylacetophenone (134 mg, 826 µmol, 1 eq) was added. After 15 min, 3,5-4-(9,9-dimethyl-9H-fluoren-2-yl)benzaldehyde (1g) (246 mg, 826 µmol, 1 eq) was added dropwise and the solution was stirred 5 h at 40 °C. Afterward, the yellow mixture was extracted three times with DCM, the organic layer was dried over Na_2SO_4 and the solvent was removed under reduced pressure. The crude product was purified by column chromatography (silica gel) using a gradient from CH to CH:DCM (1:1 v/v) as an eluent and was isolated as a yellow solid. Yield: 190 mg (52%).

^{1}H NMR (300 MHz, CD_2Cl_2) δ 7.83 – 7.61 (m, 8H), 7.51 – 7.45 (m, 1H), 7.39 – 7.31 (m, 2H), 7.23 (d, J = 16.3 Hz, 1H), 7.07 – 6.87 (m, 3H), 2.35 (s, 3H), 2.20 (s, 6H), 1.54 (s, 6H). ^{13}C NMR (76 MHz, CD_2Cl_2) δ 201.19, 154.90, 154.44, 146.33, 144.08, 141.64, 139.57, 139.41, 138.96, 138.77, 137.75, 134.45, 133.88, 129.37, 128.69, 127.93, 127.84, 127.48, 126.45, 123.07, 121.65, 120.77, 120.54, 47.35, 27.37, 21.27, 19.49.

APCI-MS m/z: calc. for $C_{33}H_{31}O$ $[M + H]^+$: 443.2, found: 443.1.

Synthesis of 2,6-bis(5-mesityl-3-phenyl-1H-pyrrol-2-yl) pyridine (H_2MesPDPPh): In a flame-dried Schlenk tube, 2,6-pyridinedicarboxaldehyde (3) (150.0 mg, 1.11 mmol, 1 eq), compound 2a (567.3 mg, 2.27 mmol, 2.04 eq) and 3-benzyl-5-(2-hydroxyethyl)-4-methylthiazolium chloride (211.7 mg, 828 µmol, 0.75 eq) were dissolved in dry EtOH (4 mL) under argon atmosphere. The solution was degassed with argon for 15 min before sodium *tert*-butoxide (80.0 mg, 832 µmol, 0.75 eq) was added during stirring. The dark brown mixture was stirred at reflux for 12 h. Subsequently, the reaction was allowed to cool to room temperature, NH_4OAc (518.0 mg, 6.72 mmol, 6 eq) was added under ambient conditions and the mixture was heated to reflux for 72 h. After cooling to room temperature, the yellow precipitate was isolated by filtration and washed three times with cold (≈0 °C) EtOH. The product was purified by column chromatography (silica gel) using a gradient from CH to CH:DCM (1:1 v/v) as an eluent and was isolated as a pale-yellow solid. Yield: 278 mg (42%).

^{1}H NMR (300 MHz, C_6D_6) δ 11.51 (s, 2H), 7.64 (d, J = 6.9 Hz, 4H), 7.39 (t, J = 7.5 Hz, 4H), 7.21 (t, J = 7.3 Hz, 2H), 6.78 (d, J = 8.1 Hz, 2H), 6.57 (s, 4H), 6.14 – 5.93 (m, 3H), 1.96 (s, 12H), 1.93 (s, 6H). ^{13}C NMR (76 MHz, C_6D_6) δ 150.42, 138.76, 138.62, 137.19, 136.53, 133.36, 130.02, 129.92, 128.82, 128.38, 128.06, 127.99, 127.74, 127.45, 126.94, 125.66, 117.74, 112.57, 21.02, 20.52.

APCI-MS m/z: calc. for $C_{43}H_{40}N_3$ $[M + H]^+$: 598.3, found: 598.4.

Synthesis of 2,6-bis(3-(4-(tert-butyl)phenyl)-5-mesityl-1H-pyrrol-2-yl)pyridine (H_2MesPDPt-BuPh): The synthesis of H_2MesPDPt-BuPh was performed analogously to H_2MesPDPPh. However, 45.0 mg (333 µmol, 1 eq) of 2,6-pyridinedicarboxaldehyde (3), 204.1 mg (666 µmol, 2 eq) of compound 2b, 63.0 mg (246 µmol, 0.75 eq) of 3-benzyl-5-(2-hydroxyethyl)-4-methylthiazolium chloride and 23.9 mg (250 µmol, 0.75 eq) of sodium *tert*-butoxide dissolved in 4 mL dry EtOH were used instead. After 24 h, the mixture was transferred to a thick-walled pressure vessel, 153.0 mg (1.98 mmol, 6 eq) of NH_4OAc was added and the mixture was heated to 170 °C for 3.5 h. The product was isolated after filtration as a yellow solid. Yield: 126 mg (53%).

^{1}H NMR (300 MHz, C_6D_6) δ 11.55 (s, 2H), 7.69 (d, J = 7.9 Hz, 4H), 7.56 (d, J = 7.9 Hz, 4H), 6.91 (d, J = 8.1 Hz, 2H), 6.58 (s, 4H), 6.15 – 5.97 (m, 3H), 2.01 (s, 12H), 1.92 (s, 6H), 1.33 (s, 18H). ^{13}C NMR (76 MHz, C_6D_6) δ 150.62, 149.48, 138.86, 137.11, 136.77, 135.74, 133.39, 130.17, 129.63, 127.24, 125.78, 125.72, 117.96, 112.62, 34.63, 31.59, 21.06, 20.57.

APCI-MS m/z: calc. for $C_{51}H_{56}N_3$ $[M + H]^+$: 710.5, found: 710.6.

Synthesis of 2,6-bis(5-mesityl-3-(3,4,5-trifluorophenyl)-1H-pyrrol-2-yl) pyridine (H_2MesPDPF3Ph): The synthesis of H_2MesPDPF3Ph was performed analogously to H_2MesPDPPh. However, 33.3 mg (246 µmol, 1 eq) of 2,6-pyridinedicarboxaldehyde (3), 150.3 mg (494 µmol, 2.05 eq) of compound 2c, 33.5 mg (124 µmol, 0.5 eq) of 3-benzyl-5-(2-hydroxyethyl)-4-methylthiazolium chloride and 11.6 mg (121 µmol, 0.5 eq) of sodium *tert*-butoxide dissolved in 4 mL dry EtOH were used instead. After 24 h, the mixture was transferred to a thick-walled pressure vessel, 125.2 mg (1.62 mmol, 6 eq) of NH_4OAc was added and the mixture was heated to 170 °C for 3.5 h. The product was isolated after filtration as a pale-yellow solid. Yield: 96 mg (56%).

^{1}H NMR (300 MHz, $CDCl_3$) δ 11.02 (s, 2H), 7.12 (t, J = 7.6 Hz, 1H), 7.00 (t, J = 7.5 Hz, 4H), 6.65 (s, 4H), 6.48 (t, J = 4.3 Hz, 2H), 5.87 (d, J = 2.6 Hz, 2H), 2.20 (s, 6H), 1.61 (s, 12H). ^{13}C NMR (76 MHz, $CDCl_3$) δ 153.23, 149.87, 149.31, 138.54, 138.25, 138.16, 136.89, 133.55, 133.26, 128.76, 127.86, 125.19, 124.22, 117.84, 113.16, 111.95, 20.96, 20.01.

APCI-MS m/z: calc. for $C_{43}H_{34}F_6N$ $[M + H]^+$: 706.3, found: 706.6.

Synthesis of 2,6-bis(5-mesityl-3-(perfluorophenyl)-1H-pyrrol-2-yl) pyridine (H_2MesPDPC6F5): The synthesis of H_2MesPDPC6F5 was performed analogously to H_2MesPDPPh. However, 62.2 mg (460 µmol, 1 eq) of 2,6-pyridinedicarboxaldehyde (3), 300.1 mg (882 µmol, 2.05 eq) of compound 2d, 81.8 mg (303 µmol, 0.7 eq) of 3-benzyl-5-(2-hydroxyethyl)-4-methylthiazolium chloride and 29.4 mg (306 µmol, 0.7 eq) of sodium

tert-butoxide dissolved in 4 mL dry EtOH were used instead. After 24 h, the mixture was transferred to a thick-walled pressure vessel, 226.4 mg (2.94 mmol, 6 eq) of NH_4OAc was added and the mixture was heated to 170 °C for 3.5 h. The product was isolated after filtration as a white solid. Yield: 139 mg (41%).

^{1}H NMR (300 MHz, $CDCl_3$) δ 9.28 (s, 2H), 7.38 (t, J = 8.0 Hz, 1H), 6.96 (s, 4H), 6.80 (d, J = 7.9 Hz, 2H), 6.13 (d, J = 3.0 Hz, 2H), 2.32 (s, 6H), 2.19 (s, 12H). ^{13}C NMR (76 MHz, $CDCl_3$) δ 149.41, 146.35, 143.02, 139.74, 138.76, 138.63, 137.52, 136.38, 131.83, 129.31, 128.60, 128.34, 115.94, 113.34, 107.01, 21.23, 20.70.

APCI-MS m/z: calc. for $C_{43}H_{30}F_{10}N_3$ $[M + H]^+$: 778.2, found: 778.5.

Synthesis of 2,6-bis(3-(3,5-bis(trifluoromethyl)phenyl)-5-mesityl-1H-pyrrol-2-yl)pyridine (H_2^{Mes}PDP^{CF3Ph}): The synthesis of H_2^{Mes}PDP^{CF3Ph} was performed analogously to H_2^{Mes}PDP^{Ph}. However, 35.8 mg (265 µmol, 1 eq) of 2,6-pyridinedicarboxaldehyde (3), 205.0 mg (531 µmol, 2 eq) of compound 2e, 51.0 mg (199 µmol, 0.75 eq) of 3-benzyl-5-(2-hydroxyethyl)-4-methylthiazolium chloride and 19.0 mg (198 µmol, 0.75 eq) of sodium *tert*-butoxide dissolved in 4 mL dry EtOH were used instead. After 24 h, the mixture was transferred to a thick-walled pressure vessel, 125.0 mg (1.62 mmol, 6 eq) of NH_4OAc was added and the mixture was heated to 170 °C for 7 h. The product was isolated after filtration as a yellow solid. Yield: 118 mg (51%).

^{1}H NMR (300 MHz, C_6D_6) δ 11.40 (s, 2H), 8.03 (s, 4H), 7.75 (s, 2H), 6.67 (s, 4H), 6.57 (d, J = 8.0 Hz, 2H), 6.29 (t, J = 8.0 Hz, 1H), 5.67 (d, J = 2.4 Hz, 2H), 2.04 (s, 6H), 1.76 (s, 12H). ^{13}C NMR (76 MHz, C_6D_6) δ 149.81, 140.31, 138.89, 138.26, 136.97, 134.49, 133.15, 132.72, 132.28, 131.84, 129.59, 128.65, 127.99, 125.86, 125.69, 124.50, 122.25, 120.71, 118.63, 117.56, 112.55, 20.66, 20.34.

APCI-MS m/z: calc. for $C_{47}H_{36}F_{12}N_3$ $[M + H]^+$: 870.3, found: 870.5.

Synthesis of 2,6-bis(3-(3,4-bis(dodecyloxy)phenyl)-5-mesityl-1H-pyrrol-2-yl)pyridine (H_2^{Mes}PDP^{DDOPh}): The synthesis of H_2^{Mes}PDP^{DDOPh} was performed analogously to H_2^{Mes}PDP^{Ph}. However, 16.0 mg (118 µmol, 1 eq) of 2,6-pyridinedicarboxaldehyde (3), 150.3 mg (243 µmol, 2.05 eq) of compound 2f, 22.7 mg (88.8 µmol, 0.75 eq) of 3-benzyl-5-(2-hydroxyethyl)-4-methylthiazolium chloride and 8.5 mg (88.8 µmol, 0.75 eq) of sodium *tert*-butoxide dissolved in 4 mL dry EtOH were used instead. After 24 h, the mixture was transferred to a thick-walled pressure vessel, 75.0 mg (973 mmol, 8 eq) of NH_4OAc was added and the mixture was heated to 170 °C for 3.5 h. The product was isolated after filtration as a yellow solid. Yield: 42 mg (27%).

^{1}H NMR (300 MHz, C_6D_6) δ 11.81 – 11.60 (m, 2H), 7.44 (d, J = 2.1 Hz, 2H), 7.34 (d, J = 8.7 Hz, 2H), 7.07 (d, J = 7.7 Hz, 4H), 6.74 (s, 4H), 6.34 (t, J = 8.0 Hz, 1H), 6.17 (d, J = 2.6 Hz, 2H), 4.09 (t, J = 6.3 Hz, 4H), 3.91 (t, J = 6.5 Hz, 4H), 2.14 (s, 12H), 2.06 (s, 6H), 1.88 (p, J = 6.0, 5.0 Hz, 4H), 1.78 (t, J = 7.4 Hz, 4H), 1.61 (d, J = 7.3 Hz, 4H), 1.50 (t, J = 7.5 Hz, 4H), 1.33 (d, J = 9.4 Hz, 64H), 0.97 – 0.92 (m, 12H). ^{13}C NMR (76 MHz, C_6D_6) δ 150.61, 150.29, 149.49, 138.92, 137.17, 136.42, 133.24, 131.61, 130.26, 128.81, 126.94, 125.66, 122.92, 117.51, 116.85, 114.64, 112.80, 70.10, 69.45, 32.40, 30.31, 30.24, 30.20, 30.12, 30.05, 29.99, 29.90, 26.84, 26.70, 23.17, 21.20, 20.79, 14.41.

APCI-MS m/z: calc. for $C_{91}H_{136}N_3O_4$ $[M + H]^+$: 1335.1, found: 1334.7.

Synthesis of 2,6-bis(3-(4-(9,9-dimethyl-9H-fluoren-2-yl)phenyl)-5-mesityl-1H-pyrrol-2-yl)pyridine (H_2^{Mes}PDP^{FluorenePh}): The synthesis of H_2^{Mes}PDP^{FluorenePh} was performed analogously to H_2^{Mes}PDP^{Ph}. However, 22.3 mg (165 µmol, 1 eq) of 2,6-pyridinedicarboxaldehyde (3), 149.7 mg (338 µmol, 2.05 eq) of compound 2g, 31.7 mg (124 µmol, 0.75 eq) of 3-benzyl-5-(2-hydroxyethyl)-4-methylthiazolium chloride and 11.9 mg (124 µmol, 0.75 eq) of sodium *tert*-butoxide dissolved in 4 mL dry EtOH were used instead. After 24 h, the mixture was transferred to a thick-walled pressure vessel, 76.3 mg (990 mmol, 6 eq) of NH_4OAc was added and the mixture was heated to 170 °C for 7.5 h. After cooling to room temperature, the solvent was removed under reduced pressure and the product was purified by column chromatography (silica gel) using a gradient from CH to CH:DCM (7:3 v/v) as an eluent. The product was isolated as a yellow solid. Yield: 35 mg (22%).

^{1}H NMR (300 MHz, C_6D_6) δ 11.66 (s, 2H), 7.87 (q, J = 7.9 Hz, 8H), 7.79 (s, 2H), 7.69 (s, 6H), 7.25 (dt, J = 8.3, 4.4 Hz, 8H), 6.71 (s, 4H), 6.31 (t, J = 8.0 Hz, 1H), 6.20 (d, J = 2.6 Hz, 2H), 2.11 (s, 12H), 1.95 (s, 6H), 1.44 (s, 12H). ^{13}C NMR (76 MHz, C_6D_6) δ 154.80, 154.30, 150.75, 140.97, 140.68, 139.46, 139.06, 138.91, 137.52, 137.39, 133.74, 130.31, 130.10, 128.19, 127.51, 127.17, 126.73, 125.95, 122.98, 121.81, 120.88, 120.51, 118.42, 112.68, 47.16, 27.32, 21.08, 20.66.

APCI-MS m/z: calc. for $C_{73}H_{64}N_3$ $[M + H]^+$: 982.5, found: 983.4.

Synthesis of Zr(^{Mes}PDP^{Ph})$_2$: A flame-dried Schlenk tube was loaded with H_2^{Mes}PDP^{Ph} (100.0 mg, 167 µmol, 1 eq) under an argon atmosphere. The Schlenk tube was transferred to a glovebox (N_2 atmosphere, O_2 < 0.5 ppm, H_2O < 0.5 ppm), and dry 1,2,4-trimethylbenzene (1 mL) was added. To the stirred yellow solution, 720 µL of a $ZrBn_4$ stock solution in dry 1,2,4-trimethylbenzene (46.5 mg mL^{-1}) were added and the Schlenk tube was removed from the glovebox. The orange solution was stirred at 140 °C for 48 h shielded from light. Subsequently, the reaction was allowed to cool to room temperature, the Schlenk tube was transferred again to the glovebox and another 300 µL of the $ZrBn_4$ stock solution was added. After stirring the reaction outside of the glovebox at 140 °C for another 24 h, the dark red solution was allowed to cool to room temperature and the solvent was removed under reduced pressure. The remaining red solid was purified by column chromatography (silica gel) using a gradient from CH to CH:toluene (5:1 v/v) as an eluent and the product was isolated as a red solid. Yield: 69 mg (63%).

^{1}H NMR (300 MHz, CD_2Cl_2) δ 7.52 (dt, J = 14.9, 7.1 Hz, 16H), 7.38 (t, J = 7.2 Hz, 4H), 6.82 (t, J = 8.1 Hz, 2H), 6.43 (s, 8H), 6.32 (d, J = 8.1 Hz, 4H), 5.77 (s, 4H), 1.94 (s, 12H), 1.78 (s, 24H). ^{13}C NMR (76 MHz, CD_2Cl_2) δ 154.45, 142.14, 139.90, 137.99, 137.14, 135.89, 131.63, 130.25, 129.59, 128.72, 128.19, 127.04, 115.29, 112.91, 22.83, 20.91.

HRMS (MALDI) m/z: $[M]^+$ calc. for $C_{86}H_{74}N_6Zr$, 1280.5022; found, 1280.5011.

Synthesis of Zr(^{Mes}PDP$^{t\text{-}BuPh}$)$_2$: The synthesis of Zr(^{Mes}PDP$^{t\text{-}BuPh}$)$_2$ was performed analogously to Zr(^{Mes}PDP^{Ph})$_2$. However, 69.3 mg (97.6 µmol, 1 eq) of H_2^{Mes}PDP$^{t\text{-}BuPh}$ dissolved in 1 mL dry 1,2,4-trimethylbenzene and 750 µL $ZrBn_4$ stock solution (29.0 mg mL^{-1}) were used instead. After 48 h, another 500 µL $ZrBn_4$ stock solution was added. The product was isolated by column chromatography (silica gel) using a gradient from CH to CH:toluene (9:1 v/v) as an eluent. Yield: 53 mg (72%).

^{1}H NMR (300 MHz, CD_2Cl_2) δ 7.50 (d, J = 1.6 Hz, 16H), 6.87 (t, J = 8.1 Hz, 2H), 6.56 – 6.36 (m, 12H), 5.74 (s, 4H), 1.99 (s, 12H), 1.76 (s, 24H), 1.43 (s, 36H). ^{13}C NMR (76 MHz, CD_2Cl_2) δ 154.71, 150.17, 142.32, 140.15, 138.94, 137.24, 135.93, 135.04, 131.92, 130.36, 129.30, 128.34, 125.83, 115.66, 113.03, 35.10, 31.81, 22.96, 21.11.

HRMS (MALDI) m/z: $[M]^+$ calc. for $C_{102}H_{106}N_6Zr$, 1504.7526; found, 1504.7573.

Synthesis of Zr(^{Mes}PDP^{F3Ph})$_2$: The synthesis of Zr(^{Mes}PDP^{F3Ph})$_2$ was performed analogously to Zr(^{Mes}PDP^{Ph})$_2$. However, 42.0 mg (59.5 µmol, 1 eq) of H_2^{Mes}PDP^{F3Ph} dissolved in 1 mL dry 1,2,4-trimethylbenzene and 320 µL $ZrBn_4$ stock solution (42.7 mg mL^{-1}) were used instead. After 48 h, another 100 µL $ZrBn_4$ stock solution was added. The product was isolated by column chromatography (silica gel) using a gradient from CH to CH:toluene (5:1 v/v) as an eluent. Yield: 23 mg (52%).

^{1}H NMR (300 MHz, CD_2Cl_2) δ 7.17 (t, J = 7.4 Hz, 8H), 6.99 (t, J = 8.1 Hz, 2H), 6.44 (s, 8H), 6.38 (d, J = 8.1 Hz, 4H), 5.78 (s, 4H), 2.00 (s, 12H), 1.70 (s, 24H). ^{13}C NMR (76 MHz, CD_2Cl_2) δ 154.09, 153.45, 150.08, 142.85, 141.12, 140.02, 139.85, 137.98, 137.80, 136.02, 133.95, 131.12, 128.40, 127.58, 115.54, 113.77, 113.42, 22.77, 20.98.

HRMS (MALDI) m/z: $[M]^+$ calc. for $C_{86}H_{62}F_{12}N_6Zr$, 1496.3892; found, 1496.3887.

Synthesis of Zr(^{Mes}PDP^{C6F5})$_2$: The synthesis of Zr(^{Mes}PDP^{C6F5})$_2$ was performed analogously to Zr(^{Mes}PDP^{Ph})$_2$. However, 71.3 mg (91.7 µmol, 1 eq) of H_2^{Mes}PDP^{C6F5} dissolved in 1 mL dry 1,2,4-trimethylbenzene and 450 µL $ZrBn_4$ stock solution (46.5 mg mL^{-1}) were used instead. After 48 h, another 200 µL $ZrBn_4$ stock solution was added. The product was isolated by column chromatography (silica gel) using a gradient from CH to CH:toluene (5:1 v/v) as an eluent. Yield: 43 mg (29%).

^{1}H NMR (300 MHz, CD_2Cl_2) δ 7.14 (t, J = 8.0 Hz, 2H), 6.38 (s, 8H), 6.00 (d, J = 8.0 Hz, 4H), 5.85 (s, 4H), 1.90 (s, 12H), 1.72 (s, 24H). ^{13}C NMR (76 MHz, CD_2Cl_2) δ 153.79, 143.52, 140.04, 140.01, 138.29, 137.77, 130.62, 128.39, 116.19, 113.85, 111.58, 23.04, 21.21.

HRMS (MALDI) *m/z*: $[M]^+$ calc. for $C_{86}H_{54}F_{20}N_6Zr$, 1640.3137; found, 1640.3137.

Synthesis of Zr(^{Mes}*PDP*^{CF3Ph}*)*$_2$: The synthesis of $Zr(^{Mes}PDP^{CF3Ph})_2$ was performed analogously to $Zr(^{Mes}PDP^{Ph})_2$. However, 75.0 mg (86.2 µmol, 1 eq) of $H_2{}^{Mes}PDP^{CF3Ph}$ dissolved in 1 mL dry 1,2,4-trimethylbenzene and 460 µL $ZrBn_4$ stock solution (42.7 mg mL^{-1}) were used instead. After 48 h, another 200 µL $ZrBn_4$ stock solution was added. The product was isolated by column chromatography (silica gel) using a gradient from CH to CH:toluene (5:1 v/v) as an eluent. Yield: 15 mg (19%).

^{1}H NMR (300 MHz, CD_2Cl_2) δ 8.03 (s, 8H), 7.95 (s, 4H), 6.95 (t, J = 8.1 Hz, 2H), 6.46 (s, 8H), 6.24 (d, J = 8.1 Hz, 4H), 5.91 (s, 4H), 1.95 (s, 12H), 1.75 (s, 24H). ^{13}C NMR (76 MHz, CD_2Cl_2) δ 154.45, 143.28, 140.10, 139.91, 139.73, 138.48, 136.25, 133.02, 132.59, 132.15, 131.71, 130.99, 129.78, 129.62, 128.59, 127.72, 126.01, 122.41, 121.21, 118.79, 115.78, 113.30, 23.13, 20.78.

HRMS (MALDI) *m/z*: $[M]^+$ calc. for $C_{94}H_{66}F_{24}N_6Zr$, 1824.4012; found, 1824.4005.

Synthesis of Zr(^{Mes}*PDP*^{DDOPh}*)*$_2$: The synthesis of $Zr(^{Mes}PDP^{DDOPh})_2$ was performed analogously to $Zr(^{Mes}PDP^{Ph})_2$. However, 55.0 mg (41.2 µmol, 1 eq) of $H_2{}^{Mes}PDP^{DDOPh}$ dissolved in 1 mL dry 1,2,4-trimethylbenzene and 370 µL $ZrBn_4$ stock solution (25.0 mg mL^{-1}) were used instead. After 48 h, another 150 µL $ZrBn_4$ stock solution was added. The product was isolated by flash chromatography using a gradient from CH to CH:toluene (5:2 v/v) as an eluent. Yield: 14 mg (25%).

^{1}H NMR (300 MHz, CD_2Cl_2) δ 7.02 (dd, J = 13.1, 8.0 Hz, 12H), 6.82 (t, J = 8.1 Hz, 2H), 6.40 (s, 8H), 6.34 (d, J = 8.0 Hz, 4H), 5.72 (s, 4H), 4.10 (dt, J = 13.9, 6.5 Hz, 16H), 2.00 – 1.81 (m, 28H), 1.76 (s, 24H), 1.43 – 1.19 (m, 138H), 0.88 (q, J = 6.3 Hz, 24H). ^{13}C NMR (76 MHz, CD_2Cl_2) δ 154.85, 149.53, 148.82, 142.03, 140.11, 138.63, 137.20, 136.08, 131.99, 130.88, 130.46, 128.45, 122.27, 115.69, 115.33, 114.53, 113.12, 70.16, 69.96, 32.54, 32.52, 30.32, 30.29, 30.26, 30.18, 30.14, 30.11, 29.98, 29.96, 26.81, 26.77, 23.31, 23.28, 21.24, 14.47.

HRMS (MALDI) *m/z*: $[M]^+$ calc. for $C_{182}H_{266}N_6O_8Zr$, 2753.9639; found, 2753.9553.

Synthesis of Zr(^{Mes}*PDP*^{FluorenePh}*)*$_2$: The synthesis of $Zr(^{Mes}PDP^{FluorenePh})_2$ was performed analogously to $Zr(^{Mes}PDP^{Ph})_2$. However, 30.0 mg (30.5 µmol, 1 eq) of $H_2{}^{Mes}PDP^{FluorenePh}$ dissolved in 1 mL dry 1,2,4-trimethylbenzene and 280 µL $ZrBn_4$ stock solution (25.0 mg mL^{-1}) were used instead. After 48 h, another 100 µL $ZrBn_4$ stock solution was added. The product was isolated by flash chromatography using a gradient from CH to CH:toluene (7:3 v/v) as an eluent. Yield: 15 mg (49%).

^{1}H NMR (300 MHz, CD_2Cl_2) δ 7.90 – 7.66 (m, 32H), 7.57 – 7.47 (m, 4H), 7.37 (ddd, J = 6.1, 3.6, 1.6 Hz, 8H), 6.93 (t, J = 8.1 Hz, 2H), 6.68 – 6.41 (m, 12H), 5.87 (s, 4H), 2.02 (s, 12H), 1.86 (s, 24H), 1.59 (s, 24H). ^{13}C NMR (76 MHz, CD_2Cl_2) δ 155.11, 154.72, 154.58, 142.55, 140.57, 140.26, 140.18, 139.39, 139.09, 137.47, 137.13, 136.24, 131.87, 130.23, 130.16, 128.49, 127.92, 127.64, 127.57, 126.49, 123.26, 121.75, 120.96, 120.61, 115.58, 113.32, 47.56, 27.65, 23.09, 21.24.

HRMS (MALDI) *m/z*: $[M]^+$ calc. for $C_{146}H_{122}N_6Zr$, 2048.8777; found, 2048.8752.

Synthesis of Zr(^{Mes}*BrPDP*$^{t\text{-}BuPh}$*)*$_2$: $Zr(^{Mes}PDP^{t\text{-}BuPh})_2$ (14.9 mg, 9.9 µmol, 1 eq) was dissolved in DCM (2 mL) and NBS (7.2 mg, 40.5 µmol, 4.1 eq) was added. The solution was stirred for 1 h at room temperature and afterward, the solvent was removed under reduced pressure. The remaining red solid was purified by column chromatography (silica gel) using a gradient from heptane to heptane:DCM (1:1 v/v) as an eluent and the product was isolated as a red solid. Yield: 13.0 mg (72%).

^{1}H NMR (300 MHz, CD_2Cl_2) δ 7.61 (d, J = 8.3 Hz, 8H), 7.44 (d, J = 8.2 Hz, 8H), 6.87 (t, J = 8.1 Hz, 2H), 6.45 (s, 8H), 6.14 (d, J = 8.1 Hz, 4H), 1.91 (s, 12H), 1.76 (s, 24H), 1.45 (s, 36H). ^{13}C NMR (76 MHz, CD_2Cl_2) δ 154.28, 151.41, 140.28, 140.19, 139.56, 138.42, 136.48, 132.00, 130.24, 129.18, 128.74, 128.60, 126.08, 114.38, 104.10, 35.26, 31.79, 22.98, 21.14.

HRMS (MALDI) *m/z*: $[M]^+$ calc. for $C_{102}H_{102}Br_4N_6Zr$, 1818.3942; found, 1818.3940.

Synthesis of Zr(^{Mes}*IPDP*$^{t\text{-}BuPh}$*)*$_2$: $Zr(^{Mes}PDP^{t\text{-}BuPh})_2$ (16.4 mg, 10.9 µmol, 1 eq) was dissolved in DCM (2 mL) and NIS (11.0 mg, 48.9 µmol, 4.5 eq) was added. The solution was stirred for 2 h at room temperature and afterward, the solvent was removed under reduced pressure. The remaining red solid was purified by column chromatography (silica gel) using a gradient from heptane to heptane:DCM (1:1 v/v) as an eluent and the product was isolated as a red solid. Yield: 18.2 mg (83%).

^{1}H NMR (300 MHz, CD_2Cl_2) δ 7.61 (d, J = 8.4 Hz, 8H), 7.40 (d, J = 8.2 Hz, 8H), 6.84 (t, J = 8.1 Hz, 2H), 6.44 (s, 8H), 6.02 (d, J = 8.1 Hz, 4H), 1.89 (s, 12H), 1.73 (s, 24H), 1.46 (s, 36H). ^{13}C NMR (76 MHz, CD_2Cl_2) δ 153.92, 151.40, 144.55, 140.14, 139.39, 138.28, 137.28, 133.64, 132.15, 130.40, 130.27, 128.77, 126.04, 114.47, 77.72, 35.26, 31.80, 23.14, 21.15.

HRMS (MALDI) *m/z*: $[M]^+$ calc. for $C_{86}H_{50}I_4F_{20}N_6Zr$, 2008.3392; found, 2008.3317.

Synthesis of Zr(^{Mes}*BrPDP*^{C6F5}*)*$_2$: $Zr(^{Mes}PDP^{C6F5})_2$ (13.1 mg, 8.0 µmol, 1 eq) was dissolved in $CHCl_3$ (2 mL) and NBS (6.2 mg, 34.8 µmol, 4.4 eq) was added. The solution was stirred for 3 h at room temperature and afterward, the solvent was removed under reduced pressure. The remaining red solid was purified by column chromatography (silica gel) using a gradient from heptane to heptane:DCM (1:1 v/v) as an eluent and the product was isolated as a red solid. Yield: 11.2 mg (71%).

^{1}H NMR (300 MHz, $CDCl_3$) δ 7.22 (d, J = 8.1 Hz, 2H), 6.39 (s, 8H), 6.02 (d, J = 8.0 Hz, 4H), 1.90 (s, 12H), 1.70 (s, 24H). ^{13}C NMR (76 MHz, $CDCl_3$) δ 153.07, 141.70, 140.02, 139.75, 138.29, 137.74, 128.16, 127.53, 113.95, 104.94, 22.50, 21.29.

HRMS (MALDI) *m/z*: $[M]^+$ calc. for $C_{86}H_{50}Br_4F_{20}N_6Zr$, 1952.9586; found, 1953.0067.

Synthesis of PVA-MAA: 1,1-Dichloroethene (15.1 mmol, 0.80 g), acrylonitrile (37.1 mmol, 3.60 g), and methacrylic acid (6.4 mmol, 0.55 g) were mixed with *tert*-butyl alcohol (6 mL) in a Schlenk tube (10 mL), and the solution was carefully deoxygenated by three freeze-pump-thaw cycles and purging with argon. AIBN (0.27 mmol, 45 mg) was added and the temperature was raised to 60 °C. After 24 h at 60 °C, the mixture was cooled to room temperature, transferred to a beaker, and the polymer was precipitated by adding brine (100 mL). The rosy-colored polymer was washed several times with water and dried under reduced pressure. Yield: 2.2 g (44%).

Synthesis of PVA-TMA: 1,1-Dichloroethene (15.1 mmol, 0.80 g), acrylonitrile (37.1 mmol, 3.60 g), and [2-(methacryloyloxy)-ethyl]-trimethylammonium chloride (80 wt.% in water, 2.8 mmol, 0.72 g) were mixed with *tert*-butyl alcohol (6 mL) in a Schlenk tube (10 mL), and the solution was carefully deoxygenated by three freeze-pump-thaw cycles and purging with argon. AIBN (0.27 mmol, 46 mg) was added and the temperature was raised to 60 °C. After 24 h at 60 °C, the mixture was cooled to room temperature and the white precipitate was washed several times with isopropanol and water and dried under reduced pressure. Yield: 1.9 g (38%).

PS Planar Sensor Foils: A "cocktail" was prepared by dissolving the dye (0.5 wt.% with respect to the polymer) and polystyrene (10 wt.% with respect to the solvent) in chloroform. The "cocktail" was knife-coated on dust-free PET support with a wet film thickness of 25 µm and the foils were dried for one day at room temperature.

PVDC-co-AN Planar Sensor Foils: Dye (1 wt.% in respect to the polymer) and PVDC-*co*-AN (10 wt.% in respect to the solvent) were dissolved in dry THF and the "cocktail" was knife-coated in a glovebox on dust-free PET support (wet film thickness of 25 µm). After drying the foil for 12 h at room temperature, the foil was transferred from the glovebox to a drying chamber and was dried for another 12 h at 70 °C. Then a scattering layer (TiO_2 powder:silicone E4:heptane, 1:1:1 w/w/w) was knife-coated over the sensing layer with a wet film thickness of 75 µm and the foil was dried in a drying chamber for 6 h at 70 °C.

PVA-MAA Nanoparticles: A "cocktail" was prepared by dissolving 0.2 mg $Zr(^{Mes}IPDP^{t\text{-}BuPh})_2$ or $Zr(^{Mes}BrPDP^{C6F5})_2$ and 20 mg PVA-MAA in 10 mL acetone:THF (9:1 v/v). Water (40 mL) was quickly added to the solution under vigorous stirring and the organic solvents were removed under reduced pressure.

PVA-TMA Nanoparticles: 20 mg PVA-TMA was pre-dissolved in 200 mg hexafluoro-2-propanol, diluted with 10 mL acetone and 0.2 mg $Zr(^{Mes}IPDP^{t\text{-}BuPh})_2$ of $Zr(^{Mes}BrPDP^{C6F5})_2$ were added. Then, water (40 mL) was quickly added to the solution under vigorous stirring and the organic solvents were removed under reduced pressure.

Samples for Two-Photon Luminescence Spectra: Dye "cocktails" with 10, 25, and 50 nmol $Zr(^{Mes}IPDP^{t\text{-}BuPh})_2$, $Zr(^{Mes}IPDP^{FluorenePh})_2$ or Rhodamine B and 20 mg PVDC-*co*-AN dissolved in 180 mg THF were prepared and knife-coated on silanized glass slides (wet film thickness of 25 µm).

Measurements: ^1H and ^{13}C-APT NMR spectra were recorded on a 300 MHz instrument from Bruker. The residual signal of the deuterated solvent was used as an internal standard.

Mass spectra for reaction monitoring and characterization of intermediates were acquired on an Expression CMS L compact mass spectrometer from Advion with an atmospheric-pressure chemical ionization (APCI) source and quadrupole mass analyzer (range 10–2000 *m*/*z*). High-resolution mass spectra of the zirconium(IV) complexes were recorded on the matrix-assisted laser desorption/ionization time-of-flight mass spectrometer (MALDI-TOF MS) Micromass MALDI micro MX from Waters.

UV–vis spectra were recorded on a CARY 50 UV–vis spectrophotometer from Varian. Luminescence spectra and relative quantum yields were recorded on a Fluorolog-3 luminescence spectrometer equipped with a NIR-sensitive R2658 photomultiplier from Hamamatsu. The measurements were performed in a screw-capped quartz cuvette from Helma. Deoxygenation of toluene solutions was performed by bubbling high-purity nitrogen (99.99999% purity) from Linde Gas through the solution for at least 20 min. In order to record the spectra of dyes in PS, the foils were placed diagonally in a quartz glass precision cuvette (10 mm) filled with a 5 wt.% aqueous Na_2SO_3.

Absolute quantum yields in polystyrene were measured under oxygen-free conditions on a Fluorolog-3 spectrometer equipped with an integrating sphere Quanta-phi. Hereby, deoxygenation was performed by using a 5 wt.% glucose solution and traces of glucose oxidase.

Luminescence decay times were measured via TCSPC on a Fluorolog-3 spectrometer equipped with a SpectraLED (λ = 456 nm) excitation source and a DeltaHub module from Horiba. Data analysis was performed on DAS-6 Analysis software from Horiba using a mono-exponential fit.

Temperature was adjusted with a Cary SPV-1 × 0 Single Cell Peltier Accessory Peltier element from Varian in combination with an F12-ED refrigerated/heating circulator from Julabo. Temperature calibration curves were fitted via an Arrhenius-type model:[91]

$$\tau = \left(k_0 + k_1 \times e^{-\frac{\Delta E_{S1-T1}}{k_B \times T}}\right)^{-1} \quad (1)$$

where k_0 is the temperature-independent decay rate for the excited-state deactivation, k_1 is a pre-exponential factor, k_B is the Boltzmann constant, $\Delta E_{S1\text{-}T1}$ is the energy gap between the first triplet and first singlet state, and T is the absolute temperature.

The photostability of the Zr complexes and TMR was evaluated with a previously described home-made set-up that uses a metal-halide lamp as an excitation source.[92]

Particle size and zeta potential from nanoparticles were recorded on a Zetasizer Nano ZS from Malvern.

Fiber-Optic Sensors and Measurements: A sensor spot was stamped out of a PVDC-*co*-AN sensor foil and fixed with a metal cap on a 1 mm optical fiber. The fiber was connected to a custom version of Firesting phase fluorometer from PyroScience that was equipped with a blue LED for excitation. The tip of the fiber was held in a double-walled glass bottle filled with either water or an aqueous 5 wt.% Na_2SO_3 solution. The temperature was adjusted by a Julabo F25-ME refrigerated/heating circulator and measured by an external Pt-100 resistance thermometer. For the seven temperature steps the corresponding average lifetime τ was calculated by the equation:

$$\tau = \frac{\tan(dphi)}{2\pi \cdot f} \quad (2)$$

where f is the modulation frequency (1.5 kHz) and *dphi* is the phase shift.

Imaging and Microfluidic Setup: Luminescence lifetime imaging was performed by using a frequency domain FLIM camera with a two-tap CMOS sensor (pco.flim) from PCO Computer Optics, equipped with a 23 mm C-Mount Schneider Kreuznach Lens Xenoplan 1.4/23-0902 lens. The nanoparticle solution was excited with a high-power LED ($\lambda_{max,em}$ = 530 nm) which was controlled by a LED hub from Omicron. A combination of a Schott OG 570 and a LEE 105 Orange filter was used in front of the camera. Images were acquired with a frequency of 2 kHz and an exposure time of 700 ms.

Aqueous dispersion of nanoparticles ($Zr(^{Mes}IPDP^{t\text{-}BuPh})_2$-PVA-MAA particles) was pumped through a rhombic chamber chip (12-0915-0194-01) from microfluidic ChipShop. For pumping a 3-port valve syringe pump (Cavro Centris Pump) equipped with a 1 mL syringe from Tecan was used. The images were recorded after 1 min at the corresponding flow rate.

The temperature of the microfluidic chip was controlled by a heating plate in combination with an F12-ED refrigerated/heating circulator from Julabo. The surface temperature of the heating plate was measured with a GMH 3710 high-precision digital thermometer equipped with a Pt-100 temperature sensing element from Greisinger.

A calibration curve (Figure S10, Supporting Information) was obtained by measuring the phase shift *dphi* of the particle solution in the microfluidic chip at defined temperatures under stagnant conditions.

Cell Culture: Human colon carcinoma (HCT116) was from ATCC, human umbilical vein endothelial cells (HUVEC) and human dental pulp stem (hDPSC) were both from Lonza, respectively PT-5025 and CC-2517. HCT116 cells were cultured in McCoy's 5A media (VWR, 392–0420) supplemented with 10% FBS (heat-inactivated) (Gibco, 10270-106) and 1 mM sodium pyruvate (Gibco, 11360-070) at 37 °C. HUVEC cells were cultured in endothelial cell growth media 2 (PromoCell, C-22011) supplemented with endothelial growth supplement mix 2 (PromoCell, C-39216). hDPSC were grown in MEM Alpha Medium + Glutamax Minimum essential medium (Gibco, 32561-029) supplemented with 10% FBS (heat-inactivated) (Gibco, 10270-106). All cell lines were cultured at 37 °C in a 5% CO_2 incubator.

At 80–90% confluency cells were detached using 0.25% trypsin- 1 mM EDTA solution and passaged using 1:10 (for HCT116) and 1:3 (for hDPSC and HUVEC) seeding ratios. For spheroid formation experiments, growth medium was also supplemented with 100 U mL^{-1} penicillin and 100 U mL^{-1} streptomycin.

Adherent cells cultures were seeded on Ibidi µ-slide 8-well or 12-well (Ibidi GmbH, Germany) pre-coated glass bottom units with a mixture of 0.07 mg mL^{-1} collagen IV/ 0.03 mg mL^{-1} poly-D-Lysine, at a density of respectively 30 000 and 45 000 cells each well and incubated overnight to allow attachment. Loading of HCT116 cells with nanoparticles was typically performed by the addition of nanoparticles at 5 µg mL^{-1} (20 µg mL^{-1} for localization) concentration in complete growth medium, overnight incubation (17 h) in a 5% CO_2 incubator at 37 °C, washing cells with PBS, and exchanging with imaging medium (phenol-free plain DMEM supplemented with 10 mM HEPES, pH 7.4, 2 mM L-glutamine, 1 mM sodium pyruvate, and 10 mM D-glucose). For the localization study, additional staining was performed by adding Cholera toxin-Alexa Fluor 488 (2 µM) or Calcein Green AM (0.1 µM). After 1 h incubation, McCoy's 5A medium was exchanged for imaging medium after washing with PBS. After staining, cells were fixed using a 4% paraformaldehyde (PFA) solution for 10 min and used for confocal microscopy on an LSM980 microscope.

Tumor spheroids were formed by seeding HCT116 on a 0.5 wt.% Lipidure-CM5206 coated 96-well U-bottom plate (Amsbio, UK) at a concentration of 10 000 and 1000 cells each well with nanoparticles (5 µg mL^{-1}) and growing for 4 days. For microscopy, spheroids were transferred on pre-coated 0.07 mg mL^{-1} collagen IV/ 0.03 mg mL^{-1} poly-D-Lysine Ibidi µ-slide 8-well (Ibidi GmbH, Germany), allowed to attach for 2 h, and imaged in Phenol red-free DMEM, as above.

Microscopy: Testing of different cell and spheroids staining conditions was performed on a widefield fluorescence inverted microscope IX81 (Olympus), equipped with motorized Z-axis control, CoolLED pE4000 (16 channels, 365–770 nm), ORCA-Flash4.0LT+ (Hamamatsu) CMOS

camera, glass warming plate Okolab, CellSens Dimension v.3 software and air objective 40×/0.6 LUCPlanFLN. The following spectral channels were used, using 25% LED power and 40 ms excitation time: GFP (ex. 490 nm/ em. 510–550 nm), TXRED (ex. 580 nm/ em. 610 nm longpass filter), and HXT (ex. 405 nm/ em. 420–460 nm).

Viability Assay: HCT116 cells (10000 cells/well) were seeded in 96-well flat-bottom plates and cell viability was measured using an MTS assay (CellTiter 96 Aqueous Non-Radioactive Cell Proliferation Assay, Promega, USA). Briefly, HCT116 cells were cultured with various concentrations of $Zr(^{Mes}IPDP^{t\text{-}BuPh})_2$-PVA-TMA nanoparticles (0, 1, 5, 10, and 20 µg mL^{-1}) and incubated overnight at 37 °C and 5% CO_2. The phenol-containing medium was exchanged with 100 µL imaging medium after washing twice with PBS, and 20 µL of the MTS/PMS solution was added to each well. Cells were incubated at 37 °C for 4 h before reading the absorbance at 490 nm using Universal Microplate Reader EL800 (Bio-TEK Instruments, Inc., VT, USA). Linearity of response was evaluated by seeding cell dilutions from 64 000 to 2000 cells per well. For each condition, 6 replicates were used. Data were analyzed using GraphPad Prism 8 software. Normality was investigated using the Shapiro-Wilk Test and data was analyzed using ordinary one-way ANOVA with Tukey's multiple comparisons tests.

Two-photon Microscopy: Two-photon microscopy was done using an inverted Zeiss LSM 880 (Zeiss, Jena) microscope coupled with a Ti-Sapphire laser (Mai Tai HP; Spectra-Physics, Santa Clara, USA) and a two-channel Big 2.0 FLIM detector, as described previously.[93] Images were collected using a water immersion C-Achroplan 32 ×/0.85 objective, at 1–5% laser power, using mosaic imaging, pixel dwell time 177.30 µs, 16 frames (256 × 256 pixels, image size 177.1 × 177.1 µm) and 570–610 nm bandpass filter. The data were processed using SPCImage software (Becker&Hickl).

Confocal and PLIM microscopy: Confocal and PLIM microscopy was performed using and inverted Zeiss LSM 980 (Zeiss, Oberkochen) microscope equipped with 20 ×/0.8 Plan Apochromat and 63 ×/1.4 C-Plan-Apochromat objectives, 488, 561, and pulsed 485 nm lasers (sequence frequency 5 kHz, an excitation pulse train of 3 µs, with 12.5 ns between the pulses and 500 pulses/pulse train), MultiHarp TCSPC module (Picoquant). Intracellular localization of PFA-fixed cells was studied using 488 nm (0.2% power, to excite CTX-Alexa Fluor 488) and 561 nm (1.5% power, to excite $Zr(^{Mes}IPDP^{t\text{-}BuPh})_2$-PVA-TMA nanoparticles) using Airyscan mode (SuperResolution: 8.6 3D auto). For PLIM, time resolution of MultiHarp was set to 10 ps*4096 channels = 40.96 ns/TCSPC channel. The data were processed in Zen Blue and Symphotime (Picoquant) software. For consistency, microscopy experiments were performed in triplicate.

Additional confocal microscopy experiments (Figure S12, Supporting Information) were performed on an inverted Stellaris 8 Falcon FLIM microscope equipped with the white-light laser, hybrid detectors, temperature-controlled incubator (Okolab), and 40 ×/1.25 HC PL APO CS2 glycerol-immersion objective. Nanoparticles were excited using 527 nm (10.65%) with emission collected at 589–700 nm (HyD X3 detector). Calcein Green was excited using 490 nm (8.46%) with emission collected at 499–570 nm (HyD S2 analog detector). Scanning speed was set at 100 Hz with a pixel dwell time of 7.69 µs.

Supporting Information

Supporting Information is available from the Wiley Online Library or from the author.

Acknowledgements

The authors would like to thank David Schuster and Torsten Mayr (Institute of Analytical Chemistry and Food Chemistry, TU Graz) for their support in the precursor synthesis and for providing microfluidic chips, respectively. The authors also would also like to thank Cicerone Tudor (Zeiss, Belgium), Steffen Burgold, Mirjam Geibel (Zeiss, Oberkochen), and Volker Buschmann (Picoquant) for help with confocal PLIM measurements. This research was supported by Austrian Science Fund FWF, grant number P32079-N37.

Conflict of Interest

The authors declare no conflict of interest.

Data Availability Statement

The data that support the findings of this study are available in the supplementary material of this article.

Keywords

imaging, microfluidics, nanoparticles, nanothermometry, optical sensors, phosphorescence lifetime imaging

Received: November 15, 2022
Revised: January 2, 2023
Published online: February 19, 2023

[1] M. Giampetraglia, B. Weigelin, *Curr. Opin. Chem. Biol.* **2021**, *63*, 200.
[2] K. Y. Zhang, Q. Yu, H. Wei, S. Liu, Q. Zhao, W. Huang, *Chem. Rev.* **2018**, *118*, 1770.
[3] M. Moßhammer, K. E. Brodersen, M. Kühl, K. Koren, *Microchim. Acta* **2019**, *186*, 126.
[4] S. M. Grist, K. L. Bennewith, K. C. Cheung, *Annu. Rev. Anal. Chem.* **2022**, *15*, 221.
[5] J. Zhou, B. del Rosal, D. Jaque, S. Uchiyama, D. Jin, *Nat. Methods* **2020**, *17*, 967.
[6] W. Shi, X. Li, H. Ma, *Angew. Chemie – Int. Ed.* **2012**, *51*, 6432.
[7] J. Madsen, I. Canton, N. J. Warren, E. Themistou, A. Blanazs, B. Ustbas, X. Tian, R. Pearson, G. Battaglia, A. L. Lewis, S. P. Armes, *J. Am. Chem. Soc.* **2013**, *135*, 14863.
[8] J. T. Hou, W. X. Ren, K. Li, J. Seo, A. Sharma, X. Q. Yu, J. S. Kim, *Chem. Soc. Rev.* **2017**, *46*, 2076.
[9] A. Fercher, S. M. Borisov, A. V. Zhdanov, I. Klimant, D. B. Papkovsky, *ACS Nano* **2011**, *5*, 5499.
[10] D. B. Papkovsky, R. I. Dmitriev, *Cell. Mol. Life Sci.* **2018**, *75*, 2963.
[11] K. P. Carter, A. M. Young, A. E. Palmer, *Chem. Rev.* **2014**, *114*, 4564.
[12] B. J. Müller, A. V. Zhdanov, S. M. Borisov, T. Foley, I. A. Okkelman, V. Tsytsarev, Q. Tang, R. S. Erzurumlu, Y. Chen, H. Zhang, C. Toncelli, I. Klimant, D. B. Papkovsky, R. I. Dmitriev, *Adv. Funct. Mater.* **2018**, *28*, 1704598.
[13] H. A. Clark, R. Kopelman, R. Tjalkens, M. A. Philbert, *Anal. Chem.* **1999**, *71*, 4837.
[14] F. Wang, Y. Han, N. Gu, *ACS Sens.* **2021**, *6*, 290.
[15] T. Bai, N. Gu, *Small* **2016**, *12*, 4590.
[16] X. D. Wang, R. J. Meier, M. Schäferling, S. Bange, J. M. Lupton, M. Sperber, J. Wegener, V. Ondrus, U. Beifuss, U. Henne, C. Klein, O. S. Wolfbeis, *Adv. Opt. Mater.* **2016**, *4*, 1854.
[17] J. S. Donner, S. A. Thompson, C. Alonso-Ortega, J. Morales, L. G. Rico, S. I. C. O. Santos, R. Quidant, *ACS Nano* **2013**, *7*, 8666.
[18] N. M. Rzechorzek, M. J. Thrippleton, F. M. Chappell, G. Mair, A. Ercole, M. Cabeleira, J. Rhodes, I. Marshall, J. S. O'neill, *Brain* **2022**, *145*, 2031.

[19] P. B. Elming, B. S. Sørensen, A. L. Oei, N. A. P. Franken, J. Crezee, J. Overgaard, M. R. Horsman, *Cancers (Basel)* **2019**, *11*, 60.
[20] M. Karnebogen, D. Singer, M. Kallerhoff, R. H. Ringert, *Thermochim. Acta* **1993**, *229*, 147.
[21] M. Kawashima, K. Bensaad, C. E. Zois, A. Barberis, E. Bridges, S. Wigfield, C. Lagerholm, R. I. Dmitriev, M. Tokiwa, M. Toi, D. B. Papkovsky, F. M. Buffa, A. L. Harris, *Cancer Metab* **2020**, *8*, 13.
[22] P. L. Silva, O. A. Savchuk, J. Gallo, L. García-Hevia, M. Bañobre-López, J. B. Nieder, *Nanoscale* **2020**, *12*, 21647.
[23] H. D. A. Santos, E. C. Ximendes, M. del C. Iglesias-de la Cruz, I. Chaves-Coira, B. del Rosal, C. Jacinto, L. Monge, I. Rubia-Rodríguez, D. Ortega, S. Mateos, J. GarcíaSolé, D. Jaque, N. Fernández, *Adv. Funct. Mater.* **2018**, *28*, 1803924.
[24] M. Quintanilla, I. García, I. De Lázaro, R. García-Alvarez, M. Henriksen-Lacey, S. Vranic, K. Kostarelos, L. M. Liz-Marzán, *Theranostics* **2019**, *9*, 7298.
[25] I. S. Singh, J. D. Hasday, *Int. J. Hyperth.* **2013**, *29*, 423.
[26] X. D. Wang, O. S. Wolfbeis, R. J. Meier, *Chem. Soc. Rev.* **2013**, *42*, 7834.
[27] K. Okabe, N. Inada, C. Gota, Y. Harada, T. Funatsu, S. Uchiyama, *Nat. Commun.* **2012**, *3*, 705.
[28] D. Ross, M. Gaitan, L. E. Locascio, *Anal. Chem.* **2001**, *73*, 4117.
[29] M. A. Bennet, P. R. Richardson, J. Arlt, A. McCarthy, G. S. Buller, A. C. Jones, *Lab Chip* **2011**, *11*, 3821.
[30] E. M. Graham, K. Iwai, S. Uchiyama, A. Prasanna De Silva, S. W. Magennis, A. C. Jones, *Lab Chip* **2010**, *10*, 1267.
[31] Z. Lu, Y. Li, W. Qiu, A. L. Rogach, S. Nagl, *ACS Appl. Mater. Interfaces* **2020**, *12*, 19805.
[32] C. Hoera, S. Ohla, Z. Shu, E. Beckert, S. Nagl, D. Belder, *Anal. Bioanal. Chem.* **2015**, *407*, 387.
[33] Y. Schaerli, R. C. Wootton, T. Robinson, V. Stein, C. Dunsby, M. A. A. Neil, P. M. W. French, A. J. DeMello, C. Abell, F. Hollfelder, *Anal. Chem.* **2009**, *81*, 302.
[34] M. Dramićanin, *Luminescence Thermometry: Methods, Materials, and Applications*, Woodhead Publishing, Sawston, UK **2018**.
[35] L. Marciniak, K. Kniec, K. Elżbieciak-Piecka, K. Trejgis, J. Stefanska, M. Dramićanin, *Coord. Chem. Rev.* **2022**, *469*, 214671.
[36] D. Jaque, F. Vetrone, *Nanoscale* **2012**, *4*, 4301.
[37] S. Arai, S. C. Lee, D. Zhai, M. Suzuki, Y. T. Chang, *Sci. Rep.* **2014**, *4*, 6701.
[38] J. Jenkins, S. M. Borisov, D. B. Papkovsky, R. I. Dmitriev, *Anal. Chem.* **2016**, *88*, 10566.
[39] S. Uchiyama, C. Gota, T. Tsuji, N. Inada, *Chem. Commun.* **2017**, *53*, 10976.
[40] N. Inada, N. Fukuda, T. Hayashi, S. Uchiyama, *Nat. Protoc.* **2019**, *14*, 1293.
[41] L. Shang, F. Stockmar, N. Azadfar, G. U. Nienhaus, *Angew. Chemie – Int. Ed.* **2013**, *52*, 11154.
[42] Y. Shen, J. Lifante, I. Zabala-Gutierrez, M. de la Fuente-Fernández, M. Granado, N. Fernández, J. Rubio-Retama, D. Jaque, R. Marin, E. Ximendes, A. Benayas, *Adv. Mater.* **2022**, *34*, 2107764.
[43] S. Kalytchuk, K. Poláková, Y. Wang, J. P. Froning, K. Cepe, A. L. Rogach, R. Zbořil, *ACS Nano* **2017**, *11*, 1432.
[44] N. Bustamante, G. Ielasi, M. Bedoya, G. Orellana, *Polymers (Basel)* **2018**, *10*, 234.
[45] G. E. Khalil, K. Lau, G. D. Phelan, B. Carlson, M. Gouterman, J. B. Callis, L. R. Dalton, *Rev. Sci. Instrum.* **2004**, *75*, 192.
[46] S. M. Borisov, O. S. Wolfbeis, *Anal. Chem.* **2006**, *78*, 5094.
[47] L. H. Fischer, S. M. Borisov, M. Schaeferling, I. Klimant, O. S. Wolfbeis, *Analyst* **2010**, *135*, 1224.
[48] J. Brübach, J. P. Feist, A. Dreizler, *Meas. Sci. Technol.* **2008**, *19*, 025602.
[49] H. Aizawa, N. Ohishi, S. Ogawa, E. Watanabe, T. Katsumata, S. Komuro, T. Morikawa, E. Toba, *Rev. Sci. Instrum.* **2002**, *73*, 3089.
[50] S. M. Borisov, K. Gatterer, I. K. Brigitte Bitschnau, *J. Phys. Chem. C* **2010**, *114*, 9118.
[51] Q. Li, Y. He, J. Chang, L. Wang, H. Chen, Y. W. Tan, H. Wang, Z. Shao, *J. Am. Chem. Soc.* **2013**, *135*, 14924.
[52] K. Xue, C. Wang, J. Wang, S. Lv, B. Hao, C. Zhu, B. Z. Tang, *J. Am. Chem. Soc.* **2021**, *143*, 14147.
[53] P. Haro-González, L. Martínez-Maestro, I. R. Martín, J. García-Solé, D. Jaque, *Small* **2012**, *8*, 2652.
[54] Y. Liu, C. Li, Z. Ren, S. Yan, M. R. Bryce, *Nat. Rev. Mater.* **2018**, *3*, 18020.
[55] Z. Yang, Z. Mao, Z. Xie, Y. Zhang, S. Liu, J. Zhao, J. Xu, Z. Chi, M. P. Aldred, *Chem. Soc. Rev.* **2017**, *46*, 915.
[56] N. R. Paisley, C. M. Tonge, Z. M. Hudson, *Front Chem* **2020**, *8*, 229.
[57] J. C. Fister, D. Rank, J. M. Harris, *Anal. Chem.* **1995**, *67*, 4269.
[58] M. N. Berberan-Santos, J. M. M. Garcia, *J. Am. Chem. Soc.* **1996**, *118*, 9391.
[59] V. Augusto, C. Baleizão, M. N. Berberan-Santos, J. P. S. Farinha, *J. Mater. Chem.* **2010**, *20*, 1192.
[60] A. Steinegger, I. Klimant, S. M. Borisov, *Adv. Opt. Mater.* **2017**, *5*, 1700372.
[61] P. W. Zach, S. A. Freunberger, I. Klimant, S. M. Borisov, *ACS Appl. Mater. Interfaces* **2017**, *9*, 38008.
[62] S. E. Zieger, A. Steinegger, I. Klimant, S. M. Borisov, *ACS Sens.* **2020**, *5*, 1020.
[63] C. J. Christopherson, D. M. Mayder, J. Poisson, N. R. Paisley, C. M. Tonge, Z. M. Hudson, *ACS Appl. Mater. Interfaces* **2020**, *12*, 20000.
[64] A. Russegger, L. Eiber, A. Steinegger, S. M. Borisov, *Chemosensors* **2022**, *10*, 91.
[65] A. Steinegger, S. M. Borisov, *ACS Omega* **2020**, *5*, 7729.
[66] Y. Zhang, J. L. Petersen, C. Milsmann, *J. Am. Chem. Soc.* **2016**, *138*, 13115.
[67] Y. Zhang, D. C. Leary, A. M. Belldina, J. L. Petersen, C. Milsmann, *Inorg. Chem.* **2020**, *59*, 14716.
[68] Y. Zhang, T. S. Lee, J. M. Favale, D. C. Leary, J. L. Petersen, G. D. Scholes, F. N. Castellano, C. Milsmann, *Nat. Chem.* **2020**, *12*, 345.
[69] B. M. Hakey, J. M. Darmon, Y. Zhang, J. L. Petersen, C. Milsmann, *Inorg. Chem.* **2019**, *58*, 1252.
[70] I. Klimant, C. Huber, G. Liebsch, G. Neurauter, A. Stangelmayer, O. S. Wolfbeis, in *New Trends Fluoresc. Spectrosc.*, Springer, Berlin, Heidelberg **2001**, 257.
[71] S. M. Borisov, I. Klimant, *Anal. Chem.* **2007**, *79*, 7501.
[72] J. Zhao, W. Wu, J. Sun, S. Guo, *Chem Soc Rev* **2013**, *42*, 5323.
[73] C. Eggeling, J. Widengren, R. Rigler, C. A. M. Seidel, *Anal. Chem.* **1998**, *70*, 2651.
[74] R. C. Scaduto, L. W. Grotyohann, *Biophys. J.* **1999**, *76*, 469.
[75] Q. Zhang, H. Kuwabara, W. J. Potscavage, S. Huang, Y. Hatae, T. Shibata, C. Adachi, *J. Am. Chem. Soc.* **2014**, *136*, 18070.
[76] V. Augusto, C. Baleizão, M. N. Berberan-Santos, J. P. S. Farinha, *J. Mater. Chem.* **2010**, *20*, 1192.
[77] P. W. Zach, S. A. Freunberger, I. Klimant, S. M. Borisov, *ACS Appl. Mater. Interfaces* **2017**, *9*, 38008.
[78] S. M. Borisov, I. Klimant, *J Fluoresc* **2008**, *18*, 581.
[79] J. Brandrup, E. H. Immergut, E. A. Grulke, *Polymer Handbook*, John Wiley & Sons Inc, New York, **1999**.
[80] R. A. Wessling, D. S. Gibbs, B. E. Obi, D. E. Beyer, P. T. DeLassus, B. A. Howell, *Encyclopedia of Polymer Science and Technology*, Wiley & Sons, Inc., Hoboken, NJ, USA, **2002**.
[81] S. M. Borisov, T. Mayr, G. Mistlberger, K. Waich, K. Koren, P. Chojnacki, I. Klimant, *Talanta* **2009**, *79*, 1322.
[82] R. I. Dmitriev, S. M. Borisov, H. Düssmann, S. Sun, B. J. Müller, J. Prehn, V. P. Baklaushev, I. Klimant, D. B. Papkovsky, *ACS Nano* **2015**, *9*, 5275.
[83] O. S. Finikova, P. Chen, Z. Ou, K. M. Kadish, S. A. Vinogradov, *J Photochem Photobiol A Chem* **2008**, *198*, 75.
[84] N. S. Makarov, M. Drobizhev, A. Rebane, *Opt. Express* **2008**, *16*, 4029.
[85] C. Xu, W. W. Webb, *J. Opt. Soc. Am. B* **1996**, *13*, 481.

[86] S. Kumar, A. Singh, V. R. Singh, J. B. George, J. Balaji, *Biophys. J.* **2016**, *111*, 1328.
[87] R. P. Briñas, T. Troxler, R. M. Hochstrasser, S. A. Vinogradov, *J. Am. Chem. Soc.* **2005**, *127*, 11851.
[88] A. Sandeep, V. K. Praveen, D. S. Shankar Rao, S. Krishna Prasad, A. Ajayaghosh, *ACS Omega* **2018**, *3*, 4392.
[89] J. Xu, Q. Zong, S. Peng, J. Liao, H. Zhao, H. Kong, J. Xu, *ChemistrySelect* **2020**, *5*, 9330.
[90] Y. Peng, Z. Li, Y. Zeng, X. Xie, H. Wang, L. Li, X. Liu, *Microchim. Acta* **2010**, *170*, 17.
[91] G. Liebsch, I. Klimant, O. S. Wolfbeis, *Adv. Mater.* **1999**, *11*, 1296.
[92] D. Pfeifer, A. Russegger, I. Klimant, S. M. Borisov, *Sens Actuators B Chem* **2020**, *304*, 127312.
[93] I. A. Okkelman, R. McGarrigle, S. O'Carroll, D. C. Berrio, K. Schenke-Layland, J. Hynes, R. I. Dmitriev, *ACS Appl Bio Mater* **2020**, *3*, 5310.